Geometric Methods for Optimal Resource Allocation in Wireless Network Localization
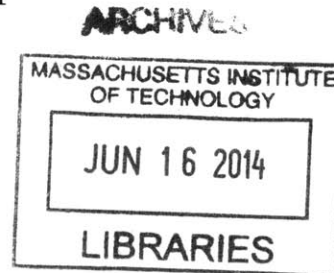
by

Wenhan Dai

Submitted to the Department of Aeronautics and Astronautics
in partial fulfillment of the requirements for the degree of

Master of Science in Aeronautics and Astronautics

at the

MASSACHUSETTS INSTITUTE OF TECHNOLOGY

June 2014

Signature redacted

Author . . . .
Department of Aeronautics and Astronautics
May 18, 2014

Signature redacted_

Certified by. . . . .
Moe Z. Win
Professor
Thesis Supervisor

Signature redacted

Accepted by . . . .
Paulo C. Lozano
Associate Professor of Aeronautics and Astronautics
Chair, Graduate Program Committee

Geometric Methods for Optimal Resource Allocation in Wireless Network Localization

by

Wenhan Dai

Submitted to the Department of Aeronautics and Astronautics
on May 18, 2014, in partial fulfillment of the
requirements for the degree of
Master of Science in Aeronautics and Astronautics

Abstract

Wireless network localization (WNL) is an emerging paradigm for providing high-accuracy positional information in GPS-challenged environments. The localization performance of a node in WNL is determined by the allocation of transmit resources among its neighboring nodes. To achieve the best localization performance, we develop a computational geometry framework for optimal resource allocation in WNL. We first determine an affine map that transforms each resource allocation strategy into a point in 3-D Euclidian space. By exploiting geometric properties of these image points, we prove the sparsity property of the optimal resource allocation vector, i.e., the optimal localization performance can be achieved by allocating resources to only a small subset of neighboring nodes. Moreover, these geometric properties enable the reduction of the search space for optimal solutions, based on which we design efficient resource allocation strategies. Numerical results show that the proposed strategies can achieve significant improvements in both localization performance and computation efficiency. Our approach provides a new methodology for resource allocation in network localization, yielding exact optimal solutions rather than ϵ-approximate solutions.

Thesis Supervisor: Moe Z. Win
Title: Professor

Acknowledgments

Contents

List of Figures

List of Tables

Chapter 1

Introduction

Wireless network localization (WNL) is a promising paradigm for providing high accuracy positional information in GPS-challenged scenarios [1–10]. Such information is crucial for many location-based applications, including logistic, security tracking, and rescuing activities [5–8, 11–16]. In WNL, there are two types of nodes, referred to as anchors and agents, where the former have known positions and the latter have unknown positions. The position of an agent can be inferred from range measurements based on wireless signals transmitted by neighboring anchors (see Fig. 1-1).

The localization performance in WNL depends on various network parameters, such as topology, signal bandwidth, channel condition, and transmit signal power [5–7, 17–21]. Among these factors, the allocation of transmit resources (e.g., power and bandwidth) plays a critical role since it not only affects network lifetime and throughput, but also determines the localization performance. Thus, it is essential to design resource allocation strategies for achieving the best localization performance [22, 23].

Extensive work has been carried out on maximizing communication and networking performance subject to resource constraints [24 30]. However, these strategies designed for data networks are not suitable for the purpose of localization since the performance metrics for localization networks are different from and more complicated than those for communication networks. Therefore, solving the resource allocation problem in WNL calls for new formulations that take into account the properties of
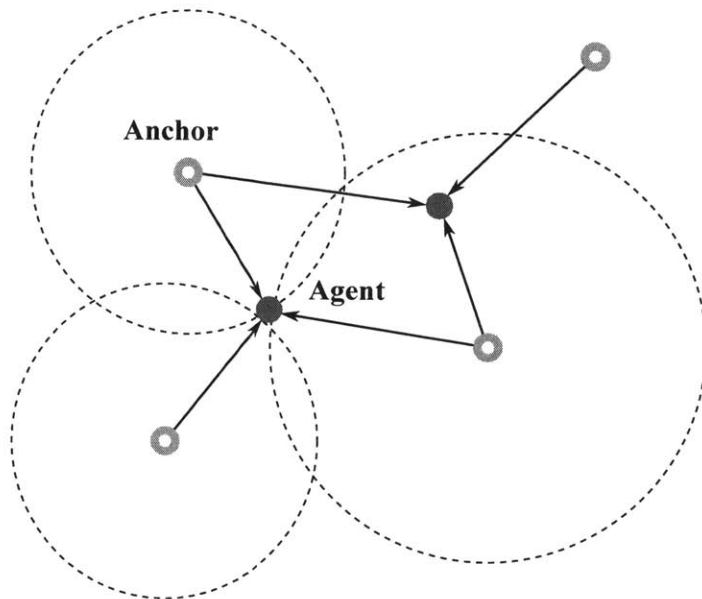
Figure 1-1: Network deployment for WNL: agents (blue dots) determine their positions based on ranging measurements with respect to anchors (red circles).

the localization performance metric [31–33]. Two fundamental questions related to resource allocation in WNL are as follows.

1. How does the localization performance depend on the resource utilization?

2. How can the available resources be optimally allocated for efficient localization?

The answers to these questions will reveal the essence of resource allocation in localization and guide the design of resource allocation strategies for WNL.

Current studies on resource allocation for localization [33–37] adopt functions of the equivalent Fisher information matrix (EFIM) as the performance metric. Typical functions include the trace of inverted EFIM [33–35, 37], and the smaller eigenvalue of the EFIM [36, 37]. These studies typically optimized the performance metric for given resource constraints and transformed the resource allocation problem into optimization programs. In [35], the power allocation problem for passive localization is investigated, where the authors employed a relaxation method and obtained suboptimal solutions. In [36], the ranging energy allocation problem for sensor positioning network is formulated as an optimization problem and a practical algorithm is proposed based on semi-definite program (SDP). In [37], the trace of inverted EFIM

and the smaller eigenvalue of the EFIM are shown as convex functions of the transmit power, and the corresponding power allocation problems for WNL are converted to conic programs. Recent work [33] unifies the power optimization problem for active and passive localization and shows that the problem can be transformed into a second-order cone program (SOCP). All these approaches obtain ϵ-approximate solutions and highly rely on optimization engines.

In this thesis, we establish a computational geometry framework for resource allocation in WNL, aiming to achieve the optimal localization performance under resource constraints. We uncover an essential property, namely low-dimensionality of the localization performance metric, leading to a linear transformation that maps each resource allocation strategy into a point in 3-D Euclidian space. This transformation enables us to exploit some geometric properties to determine the optimal resource allocation strategy. The key contributions of this thesis are as follows.

- We establish a computational geometry framework to solve resource allocation problems in WNL, exploiting the linearity and low-dimensionality of the performance metric;

- We determine the sparsity property of the optimal resource allocation vector for WNL, i.e., the optimal localization performance can be achieved by allocating resources to only a small subset of anchors;

- In the absence of individual resource constraints,[1] we develop efficient resource allocation strategies via geometric methods with computation cost $\mathcal{O}(n \log n)$ for an n-anchor network;

- In the presence of individual resource constraints, we transform the resource allocation problem into that of finding the set generated by the linear combination of vectors with bounded coefficients (LCVBC) and develop efficient algorithms with computation cost $\mathcal{O}(n^3 \log n)$.

---

[1] Individual resource constraints refer to the upper bounds for the resource consumption of *each* anchor.

The remaining chapters are organized as follows. Chapter 2 introduces the system models and the formulation for resource allocation problems. Chapter 3 presents the geometric framework and the sparsity property for optimal resource allocation vector. Chapter 4 and 5 provide the optimal solution for the resource allocation problem, in the absence of individual resource constraints. Chapter 6 presents algorithms to solve LCVBC problems and resource allocation problems with individual resource constraints. Discussions are given in Chapter 7. Finally, the efficiency and the performance gain of the proposed strategies are given in Chapter 8 and conclusions are drawn in Chapter 9.

Notation: $[\cdot]^{\mathrm{T}}$ denotes the transpose; $[\mathbf{A}]_{ij}$ denotes the element in i^{th} row and j^{th} column of matrix $\mathbf{A}$; $\mathrm{tr}\{\mathbf{A}\}$ denotes the trace of a square matrix $\mathbf{A}$; $\mathrm{rank}\{\cdot\}$ denotes the rank; $\mathbb{S}_{+}^{n}$ denotes the set of $n \times n$ positive-semidefinite matrices; $\|\mathbf{x}\|$ denotes the Euclidean norm of vector $\mathbf{x}$; $\|\mathbf{x}\|_0$ denotes the number of nonzero elements of vector $\mathbf{x}$; the relations $\mathbf{x} \succeq \mathbf{y}$ and $\mathbf{x} \succ \mathbf{y}$ denote that all elements of $\mathbf{x} - \mathbf{y}$ are nonnegative and positive, respectively; $\mathcal{CH}\{\cdot\}$ denotes the convex hull of the points; $\mathbf{I}_n$ denotes an $n \times n$ identity matrix, $\mathbf{0}_{m,n}$ denotes a $m \times n$ matrix with all 0's, and $\mathbf{1}_n$ and $\mathbf{0}_n$ denote n-dimensional vectors with all 1's and 0's, respectively, where the subscript will be omitted if clear in the context; $\mathbf{e}_k$ is a unit vector with k^{th} element being 1 and all other elements being 0's; and matrix $\mathbf{J}_r(\phi) := [\cos\phi \ \sin\phi]^{\mathrm{T}} [\cos\phi \ \sin\phi]$.

Chapter 2

Preliminaries

This chapter introduces the system model, presents the performance metric, and provides the formulation of the resource allocation problem for WNL.

2.1 System Model

Consider a wireless localization network with n anchors and multiple agents. Anchors are nodes with known positions, whereas agents are nodes with unknown positions. Each agent aims to determine its position based on range measurements made with respect to the anchors. Let $\mathcal{N}_b$ denote the set of anchors and $\mathbf{p}_k$ denote the position of anchor $k \in \mathcal{N}_b$. Without loss of generality, we focus on one agent located at $\mathbf{p}_0$ in the network. The angle and distance from anchor k to the agent are denoted by ϕ_k and d_k, respectively.

The wideband waveform received at the agent is modeled as

$$r(t) = \sum_{k \in \mathcal{N}_b} \frac{\sqrt{p_k}}{d_k^\beta} \sum_{l=1}^{L_k} \alpha_k^{(l)} s_k(t - \tau_k^{(l)}) + z_k(t)$$

where p_k is the transmit power of anchor k, β is the amplitude loss exponent, $\{s_k(t) : k \in \mathcal{N}_b\}$ is a set of orthonormal transmit wide-band waveforms, L_k is the number of multi-path components associated with the channel from anchor k to the agent, $\alpha_k^{(l)}$ and $\tau_k^{(l)}$ are the path amplitude and delay of the l-th path, respectively, and $z_k(t)$

is the additive white complex Gaussian noise process with two-side power spectral density N_0. The path delay is given by

$$\tau_k^{(l)} = \frac{1}{c_{\text{tr}}} \|\mathbf{p}_k - \mathbf{p}_0\|$$

where c_{tr} is the propagation speed of the transmit signal.

2.2   Problem Formulation

Let $\mathbf{J}_\text{e}(\mathbf{p}_0; \mathbf{x})$ denote the EFIM for $\mathbf{p}_0$, which is derived in [7] and given as[1]

$$\mathbf{J}_\text{e}(\mathbf{p}_0; \mathbf{x}) = \mathbf{J}_0 + \sum_{k \in \mathcal{N}_\text{b}} \xi_k \, x_k \, \mathbf{J}_\text{r}(\phi_k) \tag{2.1}$$

where $\mathbf{J}_0$ is the EFIM for the prior positional knowledge, x_k is the amount of resources allocated to anchor k, ξ_k is the equivalent ranging coefficient (ERC), and $\mathbf{x}$ is the resource allocation vector (RAV), denoted by

$$\mathbf{x} := \begin{bmatrix} x_1 & x_2 & \cdots & x_n \end{bmatrix}^\text{T}.$$

Equation (2.1) is general enough to accommodate different resource allocation problems in WNL, where ERCs ξ_k have different expressions depending on the choice of resource manifested in the RAV $\mathbf{x}$. Formulations for power and bandwidth allocation are given in Appendix A.1.

Any unbiased estimator $\hat{\mathbf{p}}_0$ for position $\mathbf{p}_0$ can be lower bounded by the square position error bound (SPEB) $\mathcal{P}(\mathbf{x})$, where

$$\mathcal{P}(\mathbf{x}) = \text{tr} \left\{ \mathbf{J}_\text{e}^{-1}(\mathbf{p}_0; \mathbf{x}) \right\}. \tag{2.2}$$

Since the SPEB characterizes the fundamental limit of the localization performance,

---

[1]If there is no prior positional knowledge, then $\mathbf{J}_0 = \mathbf{0}$; otherwise, (2.1) provides an approximation of the EFIM in the far field scenario. The exact form of the EFIM is discussed in Chapter 7 and we will show such approximation does not change the structure of the problem.

it will be used as a performance metric for the resource allocation problem for WNL, formulated as follows[2]

$$\mathscr{P}: \quad \min_{\{\mathbf{x}\}} \quad \mathcal{P}(\mathbf{x})$$

$$\text{s.t.} \quad \mathbf{1}^{\mathrm{T}}\mathbf{x} \leq 1 \qquad\qquad (2.3)$$

$$\mathbf{x} \succeq \mathbf{0} \qquad\qquad (2.4)$$

$$\mathbf{x} \preceq \mathbf{x}^{\mathrm{max}}. \qquad\qquad (2.5)$$

where (2.3) is the total resource constraint, (2.4) is the nonnegative constraint for resources, and (2.5) is the individual resource constraint.

Note that the methods developed in this thesis are also applicable for the problems using other performance metric (e.g., the smaller eigenvalue or the determinant of the EFIM) and some other formulations of the resource allocation problems (e.g., minimizing the total resource utilization subject to a given localization performance requirement).

2.3 Properties of SPEB

This section introduces two important properties of the SPEB.

Proposition 1 (Convexity [37]). The SPEB $\mathcal{P}(\mathbf{x})$ is a convex function of $\mathbf{x} \succeq \mathbf{0}$.

Remark 1. This proposition implies that the resource allocation problem $\mathscr{P}$ is a convex program and can be solved by convex optimization engines. In addition, the problems $\mathscr{P}$ can be transformed into SDP [37] and SOCP [33], which can be solved more efficiently than general convex programs.

Proposition 2 (Monotonicity). For two RAV $\mathbf{x}$ and $\mathbf{y}$, if $\mathbf{x} \succeq \mathbf{y}$, then $\mathcal{P}(\mathbf{x}) \leq \mathcal{P}(\mathbf{y})$.

---

[2]Solving the resource allocation problems requires the parameters such as angles and ranging coefficients (RCs). In practice, these parameters can be estimated from previous time steps in applications such as navigation and tracking. In Chapter 7, we will present a robust formulation to deal with the network parameter uncertainty.

Proof. Considering the EFIM with RAV $\mathbf{x}$ and $\mathbf{y}$, we have

$$\mathbf{J}_{\mathrm{e}}(\mathbf{p}_0; \mathbf{x}) - \mathbf{J}_{\mathrm{e}}(\mathbf{p}_0; \mathbf{y}) = \sum_{k \in \mathcal{N}_{\mathrm{b}}} (x_k - y_k)\, \xi_k \mathbf{J}_{\mathrm{r}}(\phi_k) \succeq \mathbf{0}$$

where the inequality is because $x_k \geq y_k$ and $\xi_k\, \mathbf{J}_{\mathrm{r}}(\phi_k) \in \mathbb{S}_+^2$. Since the function $\mathrm{tr}\{(\cdot)^{-1}\}$ is monotonic, we have $\mathcal{P}(\mathbf{x}) = \mathrm{tr}\{\mathbf{J}_{\mathrm{e}}^{-1}(\mathbf{p}_0; \mathbf{x})\} \leq \mathrm{tr}\{\mathbf{J}_{\mathrm{e}}^{-1}(\mathbf{p}_0; \mathbf{y})\} = \mathcal{P}(\mathbf{y})$. $\square$

Remark 2. Proposition 2 shows that the SPEB decreases with the number of resources, implying that (2.3) can be replaced with the equality $\mathbf{1}^{\mathrm{T}} \mathbf{x} = 1$. Moreover, if $\mathbf{1}^{\mathrm{T}} \mathbf{x}^{\mathrm{max}} \leq 1$, the optimal solution can be trivially obtained as $\mathbf{x} = \mathbf{x}_{\mathrm{max}}$ due to the monotonicity. Hence, we only consider the case $\mathbf{1}^{\mathrm{T}} \mathbf{x}^{\mathrm{max}} > 1$.

Chapter 3

Geometric Framework and Sparsity Property

This chapter formulates the geometric framework for resource allocation in WNL and shows the sparsity property of the optimal RAV. The problem without individual resource constraint (2.5) is first investigated, and the generalization to the problem with individual resource constraint is given in Chapter 6.

3.1   Reduced Dimension of RAV

The following proposition gives a fractional expression of the SPEB defined in (2.2).

Proposition 3. The SPEB $\mathcal{P}(\mathbf{x})$ can be written as follows

$$\mathcal{P}(\mathbf{x}) = \frac{4 \cdot y_3}{y_3^2 - y_1^2 - y_2^2}$$

where

$$y_1 = \mathbf{c}^{\mathrm{T}} \mathbf{R} \mathbf{x} - [\mathbf{J}_0]_{22} + [\mathbf{J}_0]_{11}$$

$$y_2 = \mathbf{s}^{\mathrm{T}} \mathbf{R} \mathbf{x} - 2[\mathbf{J}_0]_{12}$$

$$y_3 = \mathbf{1}^{\mathrm{T}} \mathbf{R} \mathbf{x} + \mathrm{tr}\{\mathbf{J}_0\}$$

in which $\mathbf{R} = \mathrm{diag}\{\xi_1, \xi_2, \cdots, \xi_n\}$, and

$$\mathbf{c} = \begin{bmatrix} \cos 2\phi_1 & \cos 2\phi_2 & \cdots & \cos 2\phi_n \end{bmatrix}^{\mathrm{T}}$$
$$\mathbf{s} = \begin{bmatrix} \sin 2\phi_1 & \sin 2\phi_2 & \cdots & \sin 2\phi_n \end{bmatrix}^{\mathrm{T}}.$$

Proof. The SPEB $\mathcal{P}(\mathbf{x})$ can be written as

$$\mathcal{P}(\mathbf{x}) =$$
$$\frac{4 \cdot \mathbf{1}^{\mathrm{T}} \mathbf{R}\,\mathbf{x} + 4 \cdot \mathrm{tr}\{\mathbf{J}_0\}}{\mathbf{x}^{\mathrm{T}} \mathbf{R}^{\mathrm{T}} \mathbf{\Lambda} \mathbf{R}\,\mathbf{x} + 4 \cdot \det\{\mathbf{J}_0\} + 2 \cdot \mathrm{tr}\{\mathbf{J}_0\}\mathbf{1}^{\mathrm{T}} \mathbf{R}\,\mathbf{x} + 2 \cdot ([\mathbf{J}_0]_{22} - [\mathbf{J}_0]_{11})\mathbf{c}^{\mathrm{T}} \mathbf{R}\,\mathbf{x} + 4 \cdot [\mathbf{J}_0]_{12}\,\mathbf{s}^{\mathrm{T}} \mathbf{R}\,\mathbf{x}}$$

$$(3.1)$$

where $\mathbf{\Lambda} = \mathbf{1}\,\mathbf{1}^{\mathrm{T}} - \mathbf{c}\,\mathbf{c}^{\mathrm{T}} - \mathbf{s}\,\mathbf{s}^{\mathrm{T}}$. Substituting the expression of y_1, y_2 and y_3 into (3.1), together with some algebra, gives the desired result. □

Remark 3. The following observation, essential for the design of efficient resource allocation strategies, can be made from Proposition 3: the SPEB can be written as a function of only three variables, each of which is an affine function of (possibly high-dimensional) RAV.

Consider an affine transformation that maps a RAV $\mathbf{x} \in \mathbb{R}_+^n$ to a point in 3-D space, given by

$$\mathbf{y} = \mathbf{A}\,\mathbf{x} + \mathbf{b}$$

where $\mathbf{A} = \begin{bmatrix} \mathbf{c} & \mathbf{s} & \mathbf{1} \end{bmatrix}^{\mathrm{T}} \mathbf{R}$ and

$$\mathbf{b} = \begin{bmatrix} -[\mathbf{J}_0]_{22} + [\mathbf{J}_0]_{11} & -2 \cdot [\mathbf{J}_0]_{12} & \mathrm{tr}\{\mathbf{J}_0\} \end{bmatrix}^{\mathrm{T}}.$$

Proposition 3 implies that

$$\mathcal{Q}(\mathbf{y}) := \frac{4 \cdot y_3}{y_3^2 - y_1^2 - y_2^2} = \mathcal{P}(\mathbf{x}). \tag{3.2}$$

This leads to the geometric representation of the SPEB in the next proposition.

22

Proposition 4. Given a RAV $\mathbf{x}$, $\mathbf{y} = \mathbf{A}\,\mathbf{x} + \mathbf{b}$ lies in a curve of two-sheeted hyperboloid, given by

$$\left(y_3 - 2\lambda^{-1}\right)^2 - y_1^2 - y_2^2 - 4\lambda^{-2} = 0 \tag{3.3}$$

where $\lambda = \mathcal{P}(\mathbf{x})$.

Proof. For $\lambda = \mathcal{P}(\mathbf{x})$, we have $\mathcal{Q}(\mathbf{y}) = \lambda$. Note that for a given $\lambda > 0$ and $\mathbf{y} \in \mathbb{R}^3$, $\mathcal{Q}(\mathbf{y}) = \lambda$ depicts a quadratic curve, almost identical to curve (3.3) except at $\mathbf{y} = \mathbf{0}$. $\qquad\qquad\square$

Denote the feasible RAV set and its image set, respectively, by

$$\mathcal{X} = \{\mathbf{x} \in \mathbb{R}^n : \mathbf{1}^\mathsf{T}\mathbf{x} = 1, \mathbf{0} \preceq \mathbf{x}\}$$

and

$$\mathcal{I} = \{\mathbf{y} \in \mathbb{R}^3 : \mathbf{y} = \mathbf{A}\,\mathbf{x} + \mathbf{b},\ \mathbf{x} \in \mathcal{X}\}.$$

Note that each element $\mathbf{x} \in \mathcal{X}$ can be written as a convex combination of elements in $\mathcal{E}$, where

$$\mathcal{E} = \{\mathbf{e}_1, \mathbf{e}_2, \cdots, \mathbf{e}_n\}.$$

The next proposition provides a geometric property of $\mathcal{I}$.

Proposition 5. The image set $\mathcal{I}$ is a convex polyhedron, given by $\mathcal{CH}\{\mathbf{A}\,\mathbf{e} + \mathbf{b} : \mathbf{e} \in \mathcal{E}\}$.

Proof. For any $\mathbf{x} \in \mathcal{X}$, $\mathbf{y} = \sum_{k=1}^{n} x_k(\mathbf{A}\,\mathbf{e}_k + \mathbf{b})$ with $\sum_{k=1}^{n} x_k = 1$. Thus, $\mathbf{y}$ is a convex combination of $\mathbf{A}\,\mathbf{e}_k + \mathbf{b}$, $k = 1, 2, \cdots, n$. Therefore, $\mathcal{I}$ is the convex hull of points $\mathcal{CH}\{\mathbf{A}\,\mathbf{e} + \mathbf{b} : \mathbf{e} \in \mathcal{E}\}$. $\qquad\qquad\square$

This proposition implies that for $\mathbf{x} \in \mathcal{X}$ with SPEB $\lambda = \mathcal{P}(\mathbf{x})$, $\mathbf{A}\,\mathbf{x} + \mathbf{b}$ is in the intersection of $\mathcal{I}$ and curve (3.3), as illustrated in Fig. 3-1.
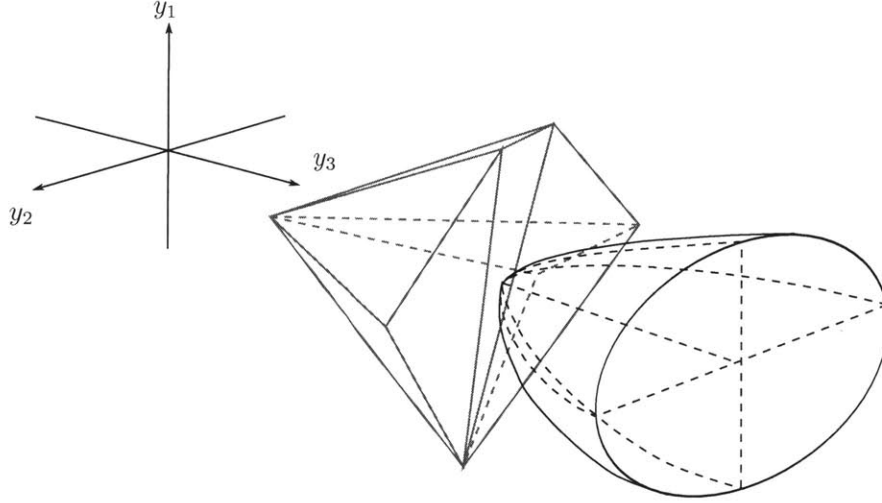
Figure 3-1: Convex polyhedron $\mathcal{I}$ and one side of two-sheeted hyperboloid prescribed by (3.3).

3.2 Geometric Properties

Based on the above geometric observations, some properties of the optimal RAV are obtained in this section.

Proposition 6. If $\mathbf{x}^*$ is an optimal solution for $\mathscr{P}$, then $\mathbf{y}^* = \mathbf{A}\,\mathbf{x}^* + \mathbf{b}$ lies on the surface of the convex polyhedron $\mathcal{I}$.

Proof. Suppose $\mathbf{y}^*$ is an interior point of $\mathcal{I}$, then there exists $\epsilon > 0$ such that $\forall \mathbf{y} \in \mathbb{R}^3$, if $\|\mathbf{y} - \mathbf{y}^*\| \leq \epsilon$, then $\mathbf{y} \in \mathcal{I}$. Let $\delta = \epsilon / (2 \cdot \|\mathbf{A}\,\mathbf{1}\|)$ and $\mathbf{x}_\delta = \mathbf{x}^* + \delta\mathbf{1}$.[1] Clearly, $|\mathbf{A}\,\mathbf{x}_\delta + \mathbf{b} - \mathbf{y}^*| \leq \epsilon$. Therefore, $\mathbf{y}_\delta = \mathbf{A}\,\mathbf{x}_\delta + \mathbf{b} \in \mathcal{I}$, and by Proposition 5, there exists $\tilde{\mathbf{x}} \in \mathcal{X}$ such that $\mathbf{y}_\delta = \sum_{k \in \mathcal{N}_\mathrm{b}} \tilde{x}_k(\mathbf{A}\,\mathbf{e}_k + \mathbf{b}) = \mathbf{A}\tilde{\mathbf{x}} + \mathbf{b}$.

Equation (3.2) gives

$$\mathcal{P}(\mathbf{x}_\delta) = \mathcal{Q}(\mathbf{A}\,\mathbf{x}_\delta + \mathbf{b})$$
$$= \mathcal{Q}(\mathbf{A}\,\tilde{\mathbf{x}} + \mathbf{b}) = \mathcal{P}(\tilde{\mathbf{x}}).$$

Since $\mathbf{x}^*$ is the optimal RAV, $\mathcal{P}(\mathbf{x}^*) \leq \mathcal{P}(\tilde{\mathbf{x}})$. Thus we have $\mathcal{P}(\mathbf{x}^*) \leq \mathcal{P}(\mathbf{x}_\delta)$. This is a contradiction since $\mathbf{x}_\delta \succ \mathbf{x}^*$, which implies that $\mathcal{P}(\mathbf{x}_\delta) < \mathcal{P}(\mathbf{x}^*)$. $\qquad\square$

---

[1] One can verify that $\mathbf{A}\,\mathbf{1} \neq \mathbf{0}$ and hence δ is well defined.

With Proposition 6, we determine the sparsity property of the optimal RAV, i.e., the optimal performance can be achieved by allocating resources to only a small subset of anchors.

Theorem 1. In 2-D networks, there exists an optimal RAV $\mathbf{x}$ for $\mathscr{P}$ such that $\|\mathbf{x}\|_0 \leq 3$.

Proof. Suppose $\mathbf{x}^*$ is an optimal solution for $\mathscr{P}$. By Proposition 6, $\mathbf{y}^* = \mathbf{A}\,\mathbf{x}^* + \mathbf{b}$ lies on the surface of $\mathcal{I}$, and hence inside a triangle with three vertices, denoted by $\mathbf{A}\,\mathbf{e}_i + \mathbf{b}$, $\mathbf{A}\,\mathbf{e}_j + \mathbf{b}$, and $\mathbf{A}\,\mathbf{e}_k + \mathbf{b}$. Thus, $\mathbf{y}^*$ can be written as a convex combination: $\mathbf{y}^* = x_i(\mathbf{A}\,\mathbf{e}_i + \mathbf{b}) + x_j(\mathbf{A}\,\mathbf{e}_j + \mathbf{b}) + x_k(\mathbf{A}\,\mathbf{e}_k + \mathbf{b})$ for nonnegative x_i, x_j and x_k such that $x_i + x_j + x_k = 1$. Let $\mathbf{x} = x_i\mathbf{e}_i + x_j\mathbf{e}_j + x_k\mathbf{e}_k$, then $\mathbf{A}\,\mathbf{x} = \mathbf{A}\,\mathbf{x}^*$ and

$$\mathcal{P}(\mathbf{x}) = \mathcal{Q}(\mathbf{A}\,\mathbf{x} + \mathbf{b})$$
$$= \mathcal{Q}(\mathbf{A}\,\mathbf{x}^* + \mathbf{b}) = \mathcal{P}(\mathbf{x}^*).$$

Hence, $\mathbf{x}$ is also an optimal solution for $\mathscr{P}$ with $\|\mathbf{x}\|_0 \leq 3$. The proof for $\mathscr{P}$ is analogous. □

Remark 4. Theorem 1 implies that the total transmit resources can be allocated to only three anchors without loss of optimality in 2-D networks. We intuit that most anchors will not be used since they either have poor channel qualities or form a relatively "bad topology." For example in Fig. 3-2, anchor 1 is not active since it is too far away from the agent compared to other anchors. Therefore, the same amount of resources allocated to other anchors contribute more in reducing the SPEB. For anchor 2, it almost forms a straight line with anchor 4, and thus, anchor 2 and anchor 4 provide information along the similar direction. However, since anchor 4 is closer to the agent, the same amount of resource in anchor 4 provides more information along the aforementioned direction and thus anchor 2 is not used.
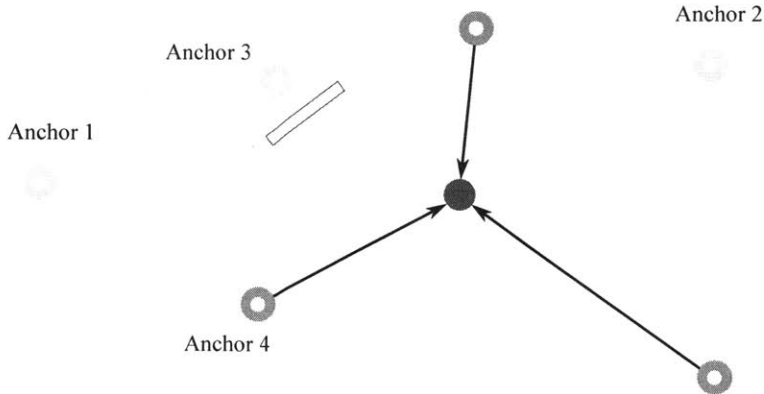
Figure 3-2: Illustration of the sparsity: the resource can be optimally allocated to only three active anchors. Most anchors will not be used due to poor channel qualities or bad topology.

3.3 Sparsity in Higher-Dimensional Localization

Theorem 1 reveals the sparsity of the optimal RAV for 2-D networks. In fact, this sparsity property is retained for networks in high dimension. Note that in high-dimensional case, the EFIM is given as

$$\mathbf{J}_{\mathrm{e}}(\mathbf{p}_0; \mathbf{x}) = \mathbf{J}_0 + \sum_{k \in \mathcal{N}_{\mathrm{b}}} \xi_k \, x_k \, \mathbf{u}_k \, \mathbf{u}_k^{\mathrm{T}} \tag{3.4}$$

where $\mathbf{u}_k = (\mathbf{p_k} - \mathbf{p}_0)/\|\mathbf{p_k} - \mathbf{p}_0\|$ and the corresponding SPEB is $\mathcal{P}(\mathbf{x}) = \mathrm{tr}\left\{\mathbf{J}_{\mathrm{e}}^{-1}(\mathbf{p}_0; \mathbf{x})\right\}$ with $\mathbf{J}_{\mathrm{e}}(\mathbf{p}_0; \mathbf{x})$ given in (3.4).

Theorem 2. There exists an optimal RAV $\mathbf{x}$ for $\mathscr{P}$ such that $\|\mathbf{x}\|_0 \leq D$ in d-dimensional networks, where $D = \binom{d+1}{2}$.

Proof. For any symmetric $d \times d$ matrix $\mathbf{M}$, we denote a one-to-one function $f \colon \mathbb{R}^{d \times d} \to \mathbb{R}^D$, such that $f(\mathbf{M})$ is a $D \times 1$ vector obtained by rearranging D elements in the upper triangular part of $\mathbf{M}$.

Note that $\mathbf{J}_{\mathrm{e}}(\mathbf{p}_0; \mathbf{x})$ is a symmetric $d \times d$ matrix, the element of which is an affine function of $\mathbf{x}$. Hence, there exists a matrix $\mathbf{B}$ and vector $\mathbf{c}$ such that $\mathbf{B}\,\mathbf{x} + \mathbf{c} = f(\mathbf{J}_{\mathrm{e}}(\mathbf{p}_0; \mathbf{x}))$. Consequently, we can rewrite the SPEB as

$$\mathcal{P}(\mathbf{x}) = \mathrm{tr}\left\{\mathbf{J}_{\mathrm{e}}^{-1}(\mathbf{p}_0; \mathbf{x})\right\}$$

26

$$= \text{tr}\left\{\left(f^{-1}(\mathbf{B}\,\mathbf{x} + \mathbf{c})\right)^{-1}\right\}$$

$$=: g(\mathbf{B}\,\mathbf{x} + \mathbf{c})$$

Let $\mathcal{J} = \{\mathbf{y} \in \mathbb{R}^D : \mathbf{y} = \mathbf{B}\,\mathbf{x} + \mathbf{c}, \mathbf{x} \in \mathcal{X}\}$. One can verify that $\mathcal{J}$ is a convex polytope, given by $\mathcal{CH}\{\mathbf{B}\,\mathbf{e}_1 + \mathbf{c}, \mathbf{B}\,\mathbf{e}_2 + \mathbf{c}, \cdots, \mathbf{B}\,\mathbf{e}_n + \mathbf{c}\}$. Similarly to Proposition 6, if $\mathbf{x}^*$ is an optimal solution for $\mathscr{P}$, then $\mathbf{y}^* = \mathbf{B}\,\mathbf{x}^* + \mathbf{c}$ lies on the boundary of the convex polytope $\mathcal{J}$, and hence inside a $(D-1)$-simplex with D vertices, denoted by $\mathbf{B}\,\mathbf{e}_{k_1} + \mathbf{c}, \mathbf{B}\,\mathbf{e}_{k_2} + \mathbf{c}, \cdots, \mathbf{B}\,\mathbf{e}_{k_D} + \mathbf{c}$. Thus, $\mathbf{y}^*$ can be written as a convex combination: $\mathbf{y}^* = \sum_{j=1}^{D} x_j (\mathbf{B}\,\mathbf{e}_{k_j} + \mathbf{c})$, for nonnegative $x_j (1 \le j \le D)$ such that $\sum_{j=1}^{D} x_j = 1$. Let $\mathbf{x} = \sum_{j=1}^{D} x_j \mathbf{e}_{k_j}$, then $\mathbf{B}\,\mathbf{x} = \mathbf{B}\,\mathbf{x}^*$ and

$$\mathcal{P}(\mathbf{x}) = g(\mathbf{B}\,\mathbf{x} + \mathbf{c})$$

$$= g(\mathbf{B}\,\mathbf{x}^* + \mathbf{c}) = \mathcal{P}(\mathbf{x}^*).$$

Hence, $\mathbf{x}$ is also an optimal solution for $\mathscr{P}$ with $\|\mathbf{x}\|_0 \le D$. $\qquad\square$

Theorem 2 is a generalization of Theorem 1. For 2-D case, a stronger result is provided as follows.

Proposition 7. For 2-D resource allocation problem $\mathscr{P}$, there exists an optimal solution $\mathbf{x}^*$ such that $\|\mathbf{x}^*\|_0 \le \text{rank}\{\boldsymbol{\Lambda}\}$.

Note that $\boldsymbol{\Lambda} = \mathbf{1}\,\mathbf{1}^\mathrm{T} - \mathbf{c}\,\mathbf{c}^\mathrm{T} - \mathbf{s}\,\mathbf{s}^\mathrm{T}$, implying $\text{rank}\{\boldsymbol{\Lambda}\} \le 3$. It can be shown that this inequality is strict for certain topologies. Consequently, Proposition 7 provides a tighter upper bound than Theorem 1. The proof for Theorem 1 and Proposition 7 via algebraic methods are shown in Appendix A.2 and Appendix A.3, respectively.

Chapter 4

Optimal RAV in Simple Networks

The sparsity property implies that the quest for the optimal resource allocation can be restricted to the small networks with three anchors, referred to as *simple networks*. This chapter presents the design of the optimal resource allocation strategies for simple networks, the understanding of which is crucial to determine the optimal RAVs for networks of arbitrary sizes.

4.1   Geometric Method for Determining the Optimal RAV

Given three feasible RAVs $\mathbf{x}_1$, $\mathbf{x}_2$ and $\mathbf{x}_3$, consider a set $\mathcal{V}$ consisting of all RAVs that can be written as a convex combination of these three RAVs, i.e.,

$$\mathcal{V} := \left\{ \mathbf{x} = \sum_{k=1}^{3} \omega_k \, \mathbf{x}_k : \sum_{k=1}^{3} \omega_k = 1, \omega_k \geq 0 \right\}.$$

The goal is to determine a RAV with smallest SPEB among this set, i.e.,

$$\mathscr{P}_{\mathrm{S}} : \quad \min_{\{\mathbf{x}\}} \quad \mathcal{P}(\mathbf{x})$$
$$\text{s.t.} \quad \mathbf{x} \in \mathcal{V}.$$

Note that the solutions of $\mathscr{P}$ can be obtained from that of $\mathscr{P}_S$ by setting $\mathbf{x}_k = \mathbf{e}_k$.

The geometric interpretation of SPEB in Proposition 4 is used to solve the problem $\mathscr{P}_S$. Let $\mathcal{U}$ denote the image set of RAVs from $\mathcal{V}$ under transformation $\mathbf{A}\,\mathbf{x} + \mathbf{b}$, i.e.,

$$\mathcal{U} := \{\mathbf{A}\,\mathbf{x} + \mathbf{b} : \mathbf{x} \in \mathcal{V}\}.$$

Clearly, $\mathcal{U}$ consists of all vectors that can be written as a convex combination of $\mathbf{u}_k = \mathbf{A}\,\mathbf{x}_k + \mathbf{b}$. Moreover, for $\lambda_1 > 0$, let

$$\mathcal{H}(\lambda_1) = \left\{\mathbf{y} \in \mathbb{R}^3 : y_1, y_2, \text{and } y_3 \text{ satisfy } (3.3)\right\}.$$

The next proposition shows that the solution of the problem $\mathscr{P}_S$ can be obtained from that of the following problem

$$\mathscr{P}_G : \quad \min_{\lambda_1 > 0} \quad \lambda_1$$
$$\text{s.t.} \quad \mathcal{U} \cap \mathcal{H}(\lambda_1) \neq \varnothing.$$

Proposition 8. For any $\mathbf{x}^\circ \in \mathcal{V}$, if $\mathbf{A}\,\mathbf{x}^\circ + \mathbf{b} \in \mathcal{H}(\lambda_1^\circ)$, where λ_1° is the optimal solution for $\mathscr{P}_G$, then $\mathbf{x}^\circ$ is an optimal solution for $\mathscr{P}_S$.

Proof. Suppose $\mathbf{x}^*$ is an optimal solution for $\mathscr{P}_S$. By Proposition 4, $\mathbf{y}^* = \mathbf{A}\,\mathbf{x}^* + \mathbf{b} \in \mathcal{H}(\lambda_1^*)$, where $\lambda_1^* = \mathcal{P}(\mathbf{x}^*)$. Clearly, $\mathbf{y}^* \in \mathcal{U}$. Hence, $\mathcal{U} \cap \mathcal{H}(\lambda_1^*) \neq \varnothing$, implying that λ_1^* is a feasible value of $\mathscr{P}_G$. Therefore, $\lambda_1^\circ \leq \lambda_1^*$ since λ_1° is the optimal value for $\mathscr{P}_G$.

It can be shown that $\mathbf{A}\,\mathbf{x}^\circ + \mathbf{b} \in \mathcal{H}(\lambda_1^\circ)$ implies $\mathcal{P}(\mathbf{x}^\circ) = \lambda_1^\circ$. Since $\mathbf{x}^\circ \in \mathcal{V}$, $\mathbf{x}^\circ$ is a feasible solution of $\mathscr{P}_S$. Therefore, $\mathcal{P}(\mathbf{x}^*) \leq \mathcal{P}(\mathbf{x}^\circ)$ since $\mathbf{x}^*$ is the optimal solution for $\mathscr{P}_S$. Equivalently, $\lambda_1^* \leq \lambda_1^\circ$. Consequently, $\mathcal{P}(\mathbf{x}^*) = \mathcal{P}(\mathbf{x}^\circ)$ and hence $\mathbf{x}^\circ$ is also an optimal solution for $\mathscr{P}_S$. $\qquad\square$

Remark 5. Note that with the optimal solution of $\mathscr{P}_G$, λ_1°, and $\mathbf{y}^\circ \in \mathcal{U} \cap \mathcal{H}(\lambda_1^\circ)$, one can obtain nonnegative ω_1°, ω_2° and ω_3° such that $\mathbf{y}^\circ = \sum_{k=1}^3 \omega_k \mathbf{u}_k$ and $\sum_{k=1}^3 \omega_k = 1$. Let $\mathbf{x}^\circ = \sum_{k=1}^3 \omega_k \mathbf{x}_k$, then one can verify that $\mathbf{x}^\circ \in \mathcal{V}$ and $\mathbf{A}\,\mathbf{x}^\circ + \mathbf{b} \in \mathcal{H}(\lambda_1^\circ)$, and hence $\mathbf{x}^\circ$ is an optimal solution for $\mathscr{P}_S$ by Proposition 8.

4.2 Optimal Solution for $\mathscr{P}_G$

The geometric method can be used to determine an optimal solution λ_1° of $\mathscr{P}_G$ and $\mathbf{y}^\circ \in \mathcal{U} \cap \mathcal{H}(\lambda_1^\circ)$. The approach of finding an optimal solution can be divided into four cases, depending on the shape of $\mathcal{U}$ and the position of $\mathbf{y}^\circ$ relative to $\mathcal{U}$.

- Case1: $\mathcal{U}$ is a triangle and $\mathbf{y}^\circ$ is an interior point of $\mathcal{U}$.

  Any point $[\,x_1\ x_2\ x_3\,]^{\mathrm{T}}$ on the plane containing $\mathcal{U}$ satisfies

  $$c_3\,x_1 + c_2\,x_2 + c_1\,x_3 + c_0 = 0$$

  where the coefficients c_k depend on $\mathcal{U}$ and assume $c_0 > 0$. Since $\mathbf{y}^\circ$ is an interior point of $\mathcal{U}$, the triangle $\mathcal{U}$ is tangent to $\mathcal{H}(\lambda_1^\circ)$ at $\mathbf{y}^\circ$. Thus, normal vectors of $\mathcal{U}$ and $\mathcal{H}(\lambda_1^\circ)$ are aligned at $\mathbf{y}^\circ$, implying that there exists t such that

  $$t\,\mathbf{c} = [\,-y_1^\circ\ \ -y_2^\circ\ \ (y_3^\circ - 2\lambda_1^{\circ-1})\,]^{\mathrm{T}}. \tag{4.1}$$

  Moreover, since $\mathbf{y}^\circ$ lies in both $\mathcal{U}$ and $\mathcal{H}(\lambda_1)$,

  $$c_3\,y_1^\circ + c_2\,y_2^\circ + c_1\,y_3^\circ + c_0 = 0$$
  $$\left(y_3^\circ - 2\lambda_1^{\circ-1}\right)^2 - y_1^{\circ 2} - y_2^{\circ 2} - 4\lambda_1^{\circ-2} = 0 \tag{4.2}$$

  Solving the equations above gives

  $$\lambda_1^\circ = \frac{2\sqrt{c_1^2 - c_2^2 - c_3^2} - 2\,c_1}{c_0} \tag{4.3}$$
  $$t = \frac{c_0 + 2c_1/\lambda_1^\circ}{c_3^2 + c_2^2 - c_1^2} \tag{4.4}$$

  and $\mathbf{y}^\circ$ can be obtained by substituting (4.3) and (4.4) into (4.1).

- Case 2: $\mathcal{U}$ is a triangle and $\mathbf{y}^\circ$ is on the edge of $\mathcal{U}$, but not a vertex of $\mathcal{U}$.

  Without loss of generality, suppose the edge containing $\mathbf{y}^\circ$ connects $\mathbf{u}_1$ and $\mathbf{u}_2$

31

and therefore $\mathbf{y}^\circ$ can be written as

$$\mathbf{y}^\circ = \mathbf{u}_1 + t\,(\mathbf{u}_1 - \mathbf{u}_2) \tag{4.5}$$

for some $t \in [\,0, 1\,]$. Let $[\,a_1\ a_2\ a_3\,]^{\mathrm{T}} = \mathbf{u}_1$ and $[\,b_1\ b_2\ b_3\,]^{\mathrm{T}} = \mathbf{u}_1 - \mathbf{u}_2$. Since $\mathbf{y}^\circ$ is an interior point of the edge, $\mathbf{u}_1 - \mathbf{u}_2$ is orthogonal to the normal vector of $\mathcal{H}$ at $\mathbf{y}^\circ$, i.e.,

$$-y_1^\circ\, b_1 - y_2^\circ\, b_2 + (y_3 - 2/\lambda_1^\circ)b_3 = 0 \tag{4.6}$$

Substituting (4.5) into (4.6) and (4.2) gives

$$A_2\, t^2 + A_1\, t + A_0 = 0 \tag{4.7}$$

where

$$A_2 = b_3\,(b_3^2 - b_2^2 - b_1^2)$$
$$A_1 = 2\, a_3\,(b_3^2 - b_2^2 - b_1^2)$$
$$A_0 = 2\, a_3\,(a_3 b_3 - a_2 b_2 - a_1 b_1) - b_3\,(a_3^2 - a_2^2 - a_1^2).$$

Then t can be solved in the closed form. The expression of $\mathbf{y}^\circ$ can be obtained accordingly.

- Case 3: $\mathcal{U}$ is a triangle and $\mathbf{y}^\circ$ is a vertex of $\mathcal{U}$.

  In this case, $\mathbf{y}^\circ$ is the vertex with the smallest λ_1.

- Case 4: $\mathcal{U}$ degenerates to a segment or a point.

  The solution can be obtained similarly to that in Case 2 or Case 3.

The observations made in the above four cases lead to Algorithm 1 for finding λ_1° and $\mathbf{y}^\circ$.

Algorithm 1 Solution to Problem $\mathscr{P}_G$

Input: $\mathcal{U}$
Output: λ_1° and $\mathbf{y}^\circ$
 1: **if** $\mathcal{U}$ is a triangle **then**
 2:     Compute λ_1 from (4.3) and the corresponding $\mathbf{y}^\circ$;
 3:     **if** $\mathbf{y}^\circ$ is in $\mathcal{U}$ **then**;
 4:         Output λ_1 and $\mathbf{y}^\circ$;
 5:     **else**
 6:         Compute λ_1 from (4.7) and the corresponding $\mathbf{y}^\circ$;
 7:         **if** $\mathbf{y}^\circ$ is in one of $\mathcal{U}$'s edges but not a vertex **then**
 8:             Output λ_1 and $\mathbf{y}^\circ$;
 9:         **else**
10:             Obtain λ_1 and $\mathbf{y}^\circ$ according to Case 3;
11:             Output λ_1 and $\mathbf{y}^\circ$;
12:         **end if**
13:     **end if**
14: **else**
15:     Obtain λ_1 and $\mathbf{y}^\circ$ according Case 4;
16: **end if**

4.3 Discussion

In resource allocation problems, Karush-Kuhn-Tucker (KKT) conditions often play an important role in determining the optimal solutions [26]. In particular, Appendix A.4 provides an alternative way of solving $\mathscr{P}$ in simple networks via checking KKT conditions.

Regardless of the specific methodology (based either on geometry or on KKT conditions), the resource allocation strategies for simple networks can be naturally extended to networks of arbitrary size based on the sparsity property. In particular, for a network of size n, there are $\binom{n}{3}$ ways to select three out of n anchors. Each combination forms a simple network, the optimal solution of which can be obtained efficiently using Algorithm 1. The optimal solution for the entire network can then be obtained by selecting the one with the minimum SPEB among all $\binom{n}{3}$ simple networks. This requires the evaluation of the SPEB for every simple network and its computation complexity is $\mathcal{O}(n^3)$. Comparatively, other strategies that obtain ϵ-approximate solutions using optimization engines (e.g., the SDP and SOCP formulation) have the worst-case computation complexity $\mathcal{O}(n^{3.5})$ [39]. The complexity of $\mathcal{O}(n^3)$ can be

further reduced by exploiting some geometric properties of the optimal RAV shown in the next chapter.

Chapter 5

Efficient Resource Allocation Strategies

This chapter presents efficient resource allocation strategies by exploiting some geometric properties shown in chapter 3.2.

5.1   Strategy via Geometric Methods

Let $\mathbf{x}^*$ be an optimal RAV for $\mathscr{P}$ (if there are multiple optimal RAVs, any one can be chosen). By Proposition 6, $\mathbf{y}^* = \mathbf{A}\mathbf{x}^* + \mathbf{b}$ lies on the surface of $\mathcal{I}$. Hence, the quest for an optimal strategy can be restricted only to those simple networks that correspond to the triangles on the surface of $\mathcal{I}$. This observation leads to Algorithm 2, which gives an optimal resource allocation strategy.

Computation complexity of Resource Allocation via Geometric Methods (RAGM): In Algorithm 2, the computation complexity of Line 1 is $\mathcal{O}(n)$. The computation complexity of Line 2 is $\mathcal{O}(n\log n)$ by using Chan's algorithm [38]. Note that the cardinality of set $\mathcal{K}$ is no greater than $(6n - 12)$ according to Proposition 9. Hence, the computation complexity for Line 3 is $\mathcal{O}(n)$ since triangulating a convex polygon with n_v vertices can be completed in time $\mathcal{O}(n_v)$ [40]. Moreover, there are no more than $6n$ cycles in the iteration from Line 4 to Line 13 and each cycle can be completed in constant time, implying that the computation complexity of the iteration is $\mathcal{O}(n)$.

Algorithm 2 Resource Allocation via Geometric Methods (RAGM)

Input: ξ_k and ϕ_k, $k \in \mathcal{N}_b$
Output: Optimal RAV $\mathbf{x}^*$ for $\mathscr{P}$

1: Initialization: $\mathbf{x}^* \leftarrow 1/n$ and $\mathcal{P}_{\text{current}} \leftarrow \mathcal{P}(1/n)$;
2: Construct $\mathcal{I} = \mathcal{CH}\{\mathbf{A}\,\mathbf{e} + \mathbf{b} : \mathbf{e} \in \mathcal{E}\}$;
3: Find a triangulation for the faces of $\mathcal{I}$ and let $\mathcal{K}$ denote the set consisted of all the resulting triangles;
4: **repeat**
5:      Find an element $K_i \in \mathcal{K}$ and let $\mathbf{A}\,\mathbf{e}_{i_1} + \mathbf{b}$, $\mathbf{A}\,\mathbf{e}_{i_2} + \mathbf{b}$ and $\mathbf{A}\,\mathbf{e}_{i_3} + \mathbf{b}$ denote the vertices of K_i;
6:      Find the optimal RAV $\widetilde{\mathbf{x}}$ according to Proposition 8 and Algorithm 1 for the simple network $\{i_1, i_2, i_3\}$;
7:      **if** $\mathcal{P}(\widetilde{\mathbf{x}}) \leq \mathcal{P}_{\text{current}}$ **then**
8:          $\mathcal{P}_{\text{current}} \leftarrow \mathcal{P}(\widetilde{\mathbf{x}})$;
9:          $\mathbf{x}^* \leftarrow \widetilde{\mathbf{x}}$;
10:      **end if**
11:      $\mathcal{K} \leftarrow \mathcal{K} \setminus \{K_i\}$;
12: **until** $\mathcal{K} = \varnothing$
13: Output $\mathbf{x}^*$.

Hence, the total computation complexity is $\mathcal{O}(n \log n)$.

Proposition 9. $|\mathcal{K}| \leq 6n - 12$.

Proof. Let E denote the number of edges of $\mathcal{I}$. Then $E \leq 3n - 6$ by Euler's formula. Let l_1, l_2, $\cdots$, l_F denote the number of edges for the faces of $\mathcal{I}$, where F is the number of faces of $\mathcal{I}$. Then

$$\sum_{k=1}^{F} l_k = 2 \cdot E \leq 6n - 12.$$

Note that a convex polygon with n_e edges can be divided into $(n_e - 2)$ triangles. Hence,

$$|\mathcal{K}| \leq \sum_{k=1}^{F} l_k \leq 6n - 12$$

which gives the desired result. $\qquad\qquad\square$

Remark 6. The initial use of geometric methods in Chapter 4.3 suggests an algorithm with computation complexity $\mathcal{O}(n^3)$ for finding an exact optimal RAV. In this section,
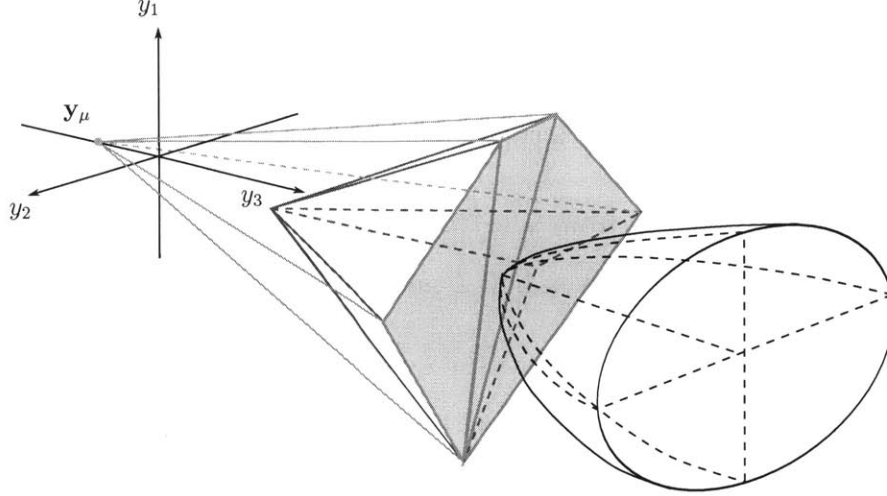
Figure 5-1: Illustration of visibility. For the optimal RAV $\mathbf{x}^*$, $\mathbf{A}\mathbf{x}^*$ lies in the red faces, which are not visible from $\mathbf{y}_\mu$.

the insight obtained from geometric methods enables the reduction of computation complexity to $\mathcal{O}(n \log n)$ without loss of optimality.

5.2 Visibility Inspired Approaches

More geometric properties can be exploited to further reduce the candidate set $\mathcal{K}$ in RAGM. Intuitively, $\mathbf{A}\mathbf{x}^* + \mathbf{b}$ belongs to the triangle facing the hyperboloid of (3.3) (the red faces in Fig. 5-1). To formalize this claim, the definition of *visible* is given as follows.

Definition 1 ([40]). *Given a convex polyhedron $\mathcal{C}$ and a point p outside $\mathcal{C}$. Let h_f denote the open half space that is generated by the plane containing a face f of $\mathcal{C}$ and does not contain $\mathcal{C}$. Then f is* visible *from the point p if p belongs to h_f.*

Consider a point $\mathbf{y}_\mu = [0, 0, \mu]^{\mathrm{T}}$ (μ is an arbitrary negative number). The next proposition shows that $\mathbf{y}^*$ lies in a face that is not visible from $\mathbf{y}_\mu$.

Proposition 10. There exists a face f^* of $\mathcal{I}$ that is not visible from $\mathbf{y}_\mu$ and contains $\mathbf{y}^*$.

Proof. See Appendix A.6. □

37

The next proposition shows that $\mathbf{y}^*$ lies on the surface of $\widetilde{\mathcal{I}}$, where $\widetilde{\mathcal{I}}$ is obtained by performing the convex hull of $\mathbf{y}_\mu$ and $\mathcal{I}$.

Proposition 11. f^* is a face of $\widetilde{\mathcal{I}}$, where $\widetilde{\mathcal{I}} = \mathcal{CH}\{\mathbf{y}_\mu, \mathbf{A}\,\mathbf{e} + \mathbf{b} : \mathbf{e} \in \mathcal{E}\}$.

Proof. Since f^* is not visible from $\mathbf{y}_\mu$, f^* lies on the surface of the new convex hull that is generated by the old convex hull $\mathcal{I}$ and the new point $\mathbf{y}_\mu$ [40]. $\qquad\square$

Remark 7. Proposition 11 implies that the quest for an optimal strategy can be performed on simple networks corresponding to triangles on the surface of $\widetilde{\mathcal{I}}$. Moreover, the search can be limited to the faces that do not contain $\mathbf{y}_\mu$ since $\mathbf{y}_\mu$ does not lie in f^*. These observations lead to Algorithm 3, which gives an optimal resource allocation strategy.

Remark 8. Resource Allocation Inspired by Visibility (RAIV) has less computation complexity than RAGM due to the following reason. In RAGM and RAIV, the complexity of generating the convex hull is $\mathcal{O}(n \log h)$, where h is the number of vertices in the output convex hull [38]. In RAGM, h is equal to n; whereas in RAIV, h is much smaller than n since many vertices of $\mathcal{I}$ become interior points of $\widetilde{\mathcal{I}}$. Moreover, the number of iterations from Line 4 to Line 13 decreases significantly since the search in RAIV is limited to faces of $\widetilde{\mathcal{I}}$ that do not contain $\mathbf{y}_\mu$. Fig. 5-2 shows the number of vertices of the output convex hulls $\mathcal{I}$ and $\widetilde{\mathcal{I}}$, and the cardinality of the triangle sets $\mathcal{K}$ and $\widetilde{\mathcal{K}}$ (i.e., the number of iterations from Line 4 to Line 13) as a function of the number of anchors.[1] It can be observed that both the number of vertices of $\mathcal{I}$ and the cardinality of $\mathcal{K}$ increase linearly with respect to n. Moreover, the number of vertices of $\widetilde{\mathcal{I}}$ and the cardinality of $\widetilde{\mathcal{K}}$ almost remain a constant as n increases. Such observation demonstrates the improvement of the efficiency of RAIV.

---

[1]Consider that an agent and anchors are placed randomly in the square region with uniform distribution. The scenario setting is the same as the one used by Case 1, in Chapter 8.2.
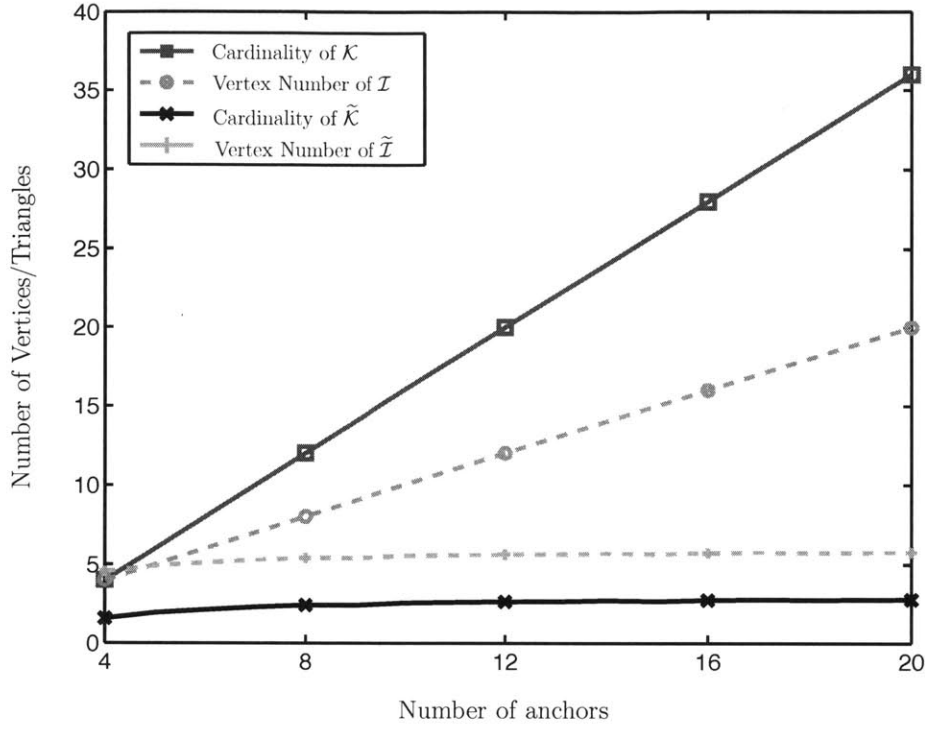
Figure 5-2: Vertex number of $\mathcal{I}$ and $\widetilde{\mathcal{I}}$ and cardinality of $\mathcal{K}$ and $\widetilde{\mathcal{K}}$.

Algorithm 3 Resource Allocation Inspired by Visibility (RAIV)

Input: ξ_k and ϕ_k, $k \in \mathcal{N}_b$
Output: Optimal RAV $\mathbf{x}^*$ for $\mathscr{P}$

1: Initialization: $\mathbf{y}_\mu \leftarrow (0, 0, \mu)$ where $\mu < 0$ and $|\mu|$ is sufficiently large; $\mathbf{x}^* \leftarrow \mathbf{1}/n$ and $\mathcal{P}_{\text{current}} \leftarrow \mathcal{P}(\mathbf{1}/n)$;
2: Construct $\widetilde{\mathcal{I}} = \mathcal{CH}\{\mathbf{y}_\mu, \mathbf{A}\,\mathbf{e} + \mathbf{b} : \mathbf{e} \in \mathcal{E}\}$;
3: Find a triangulation for the faces of $\widetilde{\mathcal{I}}$ that do not contain the point $\mathbf{y}_\mu$ and let $\widetilde{\mathcal{K}}$ denote the set consisted of all the resulting triangles;
4: **repeat**
5:     Find an element $K_i \in \widetilde{\mathcal{K}}$ and let $\mathbf{A}\,\mathbf{e}_{i_1} + \mathbf{b}$, $\mathbf{A}\,\mathbf{e}_{i_2} + \mathbf{b}$ and $\mathbf{A}\,\mathbf{e}_{i_3} + \mathbf{b}$ denote the vertices of K_i;
6:     Find the optimal RAV $\widetilde{\mathbf{x}}$ according to Proposition 8 and Algorithm 1 for the simple network $\{i_1, i_2, i_3\}$;
7:     **if** $\mathcal{P}(\widetilde{\mathbf{x}}) \leq \mathcal{P}_{\text{current}}$ **then**
8:         $\mathcal{P}_{\text{current}} \leftarrow \mathcal{P}(\widetilde{\mathbf{x}})$;
9:         $\mathbf{x}^* \leftarrow \widetilde{\mathbf{x}}$;
10:     **end if**
11:     $\widetilde{\mathcal{K}} \leftarrow \widetilde{\mathcal{K}} \setminus \{K_i\}$;
12: **until** $\widetilde{\mathcal{K}} = \varnothing$
13: Output $\mathbf{x}^*$.

Chapter 6

Resource Allocation with Individual Constraints

This chapter provides the optimal strategies for the resource allocation problem with individual constraint (2.5).

6.1 Dimension Augmentation and Projection

Denote the feasible RAV set and its image set, respectively, by

$$\mathcal{X}_{\mathrm{I}} = \{\mathbf{x} \in \mathbb{R}^n : \mathbf{1}^{\mathrm{T}} \mathbf{x} = 1, \mathbf{0} \preceq \mathbf{x} \preceq \mathbf{x}^{\max}\}$$

and

$$\mathcal{I}_{\mathrm{e}} = \{\mathbf{y} \in \mathbb{R}^3 : \mathbf{y} = \mathbf{A}\,\mathbf{x} + \mathbf{b}, \mathbf{x} \in \mathcal{X}_{\mathrm{I}}\}. \tag{6.1}$$

For $k \in \mathcal{N}_{\mathrm{b}}$, x_k has two boundary constraints $x_k \geq 0$ and $x_k \leq \mathbf{x}_k^{\max}$. Note that each element $\mathbf{x} \in \mathcal{X}_{\mathrm{I}}$ can be written as a convex combination of elements in $\mathcal{E}_{\mathrm{I}}$, where

$$\mathcal{E}_{\mathrm{I}} = \{\mathbf{x} \in \mathbb{R}^n : \mathbf{1}^{\mathrm{T}} \mathbf{x} = 1 \text{ and at least } (n - 1) \text{ boundary constraints are active}\}.$$

Similarly to Proposition 5, the next proposition provides a geometric property of $\mathcal{I}_{\mathrm{e}}$.

41

Proposition 12. The image set $\mathcal{I}_e$ is a convex polyhedron, given by $\mathcal{CH}\{\mathbf{A}\,\mathbf{e} + \mathbf{b} : \mathbf{e} \in \mathcal{E}_I\}$.

Proposition 12 can be proved similarly to Proposition 5. One can also verify that if $\mathbf{x}^*$ is the optimal solution for $\mathcal{P}$, then $\mathbf{A}\,\mathbf{x}^* + \mathbf{b}$ lies on the surface of $\mathcal{I}_e$. Therefore, the quest for the optimal strategy of $\mathcal{P}$ can be restricted to the strategies that correspond to the surface of $\mathcal{I}_e$. However, the complexity of determining the surface of $\mathcal{I}_e$ via generating the convex hull of $\{\mathbf{A}\,\mathbf{e} + \mathbf{b} : \mathbf{e} \in \mathcal{E}_I\}$ is exponential with respect to n because $\mathcal{E}_I$ has $\mathcal{O}(n \cdot 2^{n-1})$ vertices. Hence, an efficient method to determine $\mathcal{I}_e$ is required.

Consider a new affine transformation that maps a RAV $\mathbf{x} \in \mathbb{R}_+^n$ to a point in 4-D space, given by

$$\mathbf{y}_e = \mathbf{A}_e\,\mathbf{x} + \mathbf{b}_e$$

where

$$\mathbf{A}_e = \begin{bmatrix} \mathbf{A} \\ \mathbf{1}_n^T \end{bmatrix} \text{ and } \mathbf{b}_e = \begin{bmatrix} \mathbf{b} \\ 0 \end{bmatrix}.$$

Note that $\mathcal{I}_e$ in (6.1) can be written as

$$
\begin{aligned}
\mathcal{I}_e &= \left\{ \mathbf{y} : \begin{bmatrix} \mathbf{y} \\ y_0 \end{bmatrix} = \begin{bmatrix} \mathbf{A}\,\mathbf{x} + \mathbf{b} \\ \mathbf{1}^T\mathbf{x} \end{bmatrix}, \mathbf{x} \in \mathcal{X}_I \right\} \\
&= \left\{ \mathbf{y} : \begin{bmatrix} \mathbf{y} \\ y_0 \end{bmatrix} = \begin{bmatrix} \mathbf{A}_e\,\mathbf{x} + \mathbf{b}_e \end{bmatrix}, y_0 = 1, 0 \preceq \mathbf{x} \preceq \mathbf{x}^{\max} \right\} \\
&= \left\{ \mathbf{y} : \begin{bmatrix} \mathbf{y} \\ y_0 \end{bmatrix} \in \mathcal{X}_F \cap \mathcal{I}_F \right\}
\end{aligned}
$$

where

$$\mathcal{X}_F = \{\mathbf{A}_e\,\mathbf{x} + \mathbf{b}_e : 0 \preceq \mathbf{x} \preceq \mathbf{x}^{\max}\} \qquad (6.2)$$
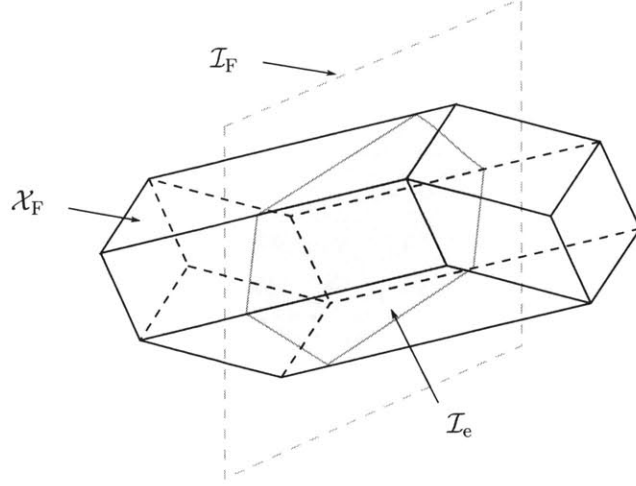
Figure 6-1: An illustration of the relationship among $\mathcal{I}_\mathrm{e}$, $\mathcal{X}_\mathrm{F}$ and $\mathcal{I}_\mathrm{F}$. $\mathcal{I}_\mathrm{e}$ (red part) is the projection of $\mathcal{X}_\mathrm{F} \cap \mathcal{I}_\mathrm{F}$ onto $\mathbb{R}^3$.

$$
\mathcal{I}_\mathrm{F} = \left\{ \begin{bmatrix} \mathbf{y} \\ 1 \end{bmatrix} : \mathbf{y} \in \mathbb{R}^3 \right\}.
$$

The relationship between $\mathcal{I}_\mathrm{e}$, $\mathcal{X}_\mathrm{F}$ and $\mathcal{I}_\mathrm{F}$ is illustrated in Fig. 6-1.

Such observation provides an alternative way to determine the surface of $\mathcal{I}_\mathrm{e}$: one can first generate $\mathcal{X}_\mathrm{F}$ and intersect it with $\mathcal{I}_\mathrm{F}$; the resulting polytope is a 3-facet, whose projection onto $\mathbb{R}^3$ is $\mathcal{I}_\mathrm{e}$. Therefore, it is sufficient to determine the edges of $\mathcal{X}_\mathrm{F}$ in order to determine $\mathcal{I}_\mathrm{e}$. Note that $\mathcal{X}_\mathrm{F}$ in (6.2) can be written as

$$
\begin{aligned}
\mathcal{X}_\mathrm{F} &= \left\{ \left(\sum_{k=1}^{n} x_k \boldsymbol{\alpha}_k \right) + \mathbf{b}_\mathrm{e}, \, 0 \le x_k \le \mathbf{x}_k^{\max} \right\} \\
&= \left\{ \mathbf{z} + \mathbf{b}_\mathrm{e} : \mathbf{z} = \sum_{k=1}^{n} x_k \boldsymbol{\alpha}_k, \, 0 \le x_k \le \mathbf{x}_k^{\max} \right\}
\end{aligned}
$$

where $\boldsymbol{\alpha}_k = [\, \xi_k \cos 2\phi_k \quad \xi_k \sin 2\phi_k \quad \xi_k \quad 1\,]^\mathrm{T}$. The edges of $\mathcal{X}_\mathrm{F}$ can be determined by solving the LCVBC problem, shown as follows.

43
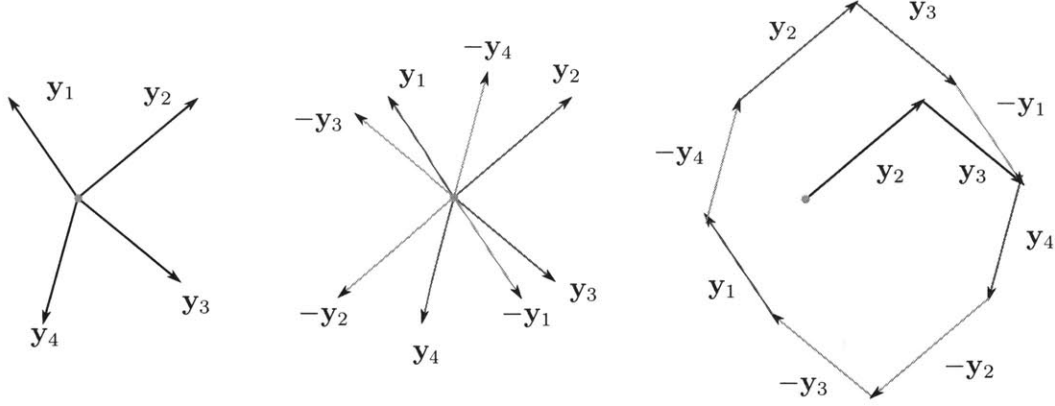
Figure 6-2: Illustration of LCVBC in 2-D space. Connecting vectors $(\mathbf{y}_1, -\mathbf{y}_4, \mathbf{y}_2, \mathbf{y}_3, -\mathbf{y}_1, \mathbf{y}_4, -\mathbf{y}_2, -\mathbf{y}_3)$ gives the polygon $\widetilde{\mathcal{I}}_{\mathrm{B}}$. The rightmost point of $\mathcal{I}_{\mathrm{B}}$ is $\mathbf{y}_{\mathrm{R}} = \mathbf{y}_2 + \mathbf{y}_3$.

6.2   LCVBC Problem

LCVBC Problem: Given N vectors $\mathbf{y}_1, \mathbf{y}_2, \cdots, \mathbf{y}_N \in \mathbb{R}^d$, the goal is to determine the vertices and edges of polytope $\mathcal{I}_{\mathrm{B}}$, given by $\mathcal{I}_{\mathrm{B}} = \left\{ \sum_{k=1}^{N} c_k \mathbf{y}_k : 0 \leq c_k \leq 1 \right\}$.

Without loss of generality, we assume that vectors $\mathbf{y}_1, \mathbf{y}_2, \cdots, \mathbf{y}_N$ are not parallel to each other. It can be shown that any vertex $\mathbf{y}$ of $\mathcal{I}_{\mathrm{B}}$ can be written as $\mathbf{y} = \sum_{i=1}^{N} w_k \mathbf{y}_k$, where $w_k \in \{0, 1\}$ is the *weight* for $\mathbf{y}_k$. Therefore, determining the edges of $\mathcal{I}_{\mathrm{B}}$ is equivalent to finding two vertices and their corresponding weights for each edge of $\mathcal{I}_{\mathrm{B}}$. Let $\mathcal{W} = \left\{ \{w_k\}_{k=1}^{N} : \sum_{i=1}^{N} w_k \mathbf{y}_k \text{ is a vertex of } \mathcal{I}_{\mathrm{B}} \right\}$ denote the weight set whose elements correspond to particular vertices of $\mathcal{I}_{\mathrm{B}}$.

6.2.1   2-D Case ($d = 2$)

Without loss of generality, we assume none of vectors $\mathbf{y}_1, \mathbf{y}_2, \cdots, \mathbf{y}_N$ is parallel to the vertical axis. $\mathcal{I}_{\mathrm{B}}$ is determined by Algorithm 4. The process can be divided into two major steps: Line 1 to Line 3 determine the relative position of $\mathcal{I}_{\mathrm{B}}$; Line 4 to Line 6 find the absolute position of $\mathcal{I}_{\mathrm{B}}$. Fig. 6-2 provides an illustration of the proposed algorithm. We claim that Algorithm 4 obtains the desired $\mathcal{I}_{\mathrm{B}}$ and the proof is given in Appendix A.7.

Algorithm 4 Linear Combination with Bounded Coefficients: 2-D Case
---
Input: N vectors in $\mathbb{R}^2$: $\mathbf{y}_1, \mathbf{y}_2, \cdots, \mathbf{y}_N$

Output: Vertices and edges of $\mathcal{I}_B$: for each edge, determine its two vertices and their corresponding weights

1: Find vectors $-\mathbf{y}_1, -\mathbf{y}_2, \cdots, -\mathbf{y}_N$;
2: Label the $2N$ vectors $\mathbf{y}_1, -\mathbf{y}_1, \mathbf{y}_2, -\mathbf{y}_2, \cdots, \mathbf{y}_N, -\mathbf{y}_N$ in a clockwise order, denoted as $\mathbf{y}^{(1)}, \mathbf{y}^{(2)}, \cdots, \mathbf{y}^{(2N)}$;
3: Connect $\mathbf{y}^{(1)}, \mathbf{y}^{(2)}, \cdots, \mathbf{y}^{(2N)}$, resulting in a polygon $\widetilde{\mathcal{I}}_B$;
4: Among vectors $\mathbf{y}_1, \mathbf{y}_2, \cdots, \mathbf{y}_N$, search the vectors with positive x components;
5: Sum up these vectors to obtain a point, denoted as $\mathbf{y}_R$;
6: Translate $\widetilde{\mathcal{I}}_B$ by $\mathbf{y}_R - \widetilde{\mathbf{y}}_R$, where $\widetilde{\mathbf{y}}_R$ denotes the rightmost vertex of $\widetilde{\mathcal{I}}_B$;
7: Output the vertices and the edges of the resulting polygon.

6.2.2 General Cases ($d > 2$)

$\mathcal{I}_B$ can be determined by induction on d. The base case ($d = 2$) has been solved by Algorithm 4. Building on that, the higher dimensional cases can be solved. For ease of exposition, the induction method is demonstrated only for $d = 3$.

One can show that each edge of $\mathcal{I}_B$ is parallel to one of the vectors $\mathbf{y}_1, \mathbf{y}_2, \cdots, \mathbf{y}_N$. We first determine those edges that are parallel to $\mathbf{y}_1$ as follows:

- Generate a normal plane $\mathcal{I}_n^1$ of vector $\mathbf{y}_1$;

- Project vectors $\mathbf{y}_2$ to $\mathbf{y}_N$ onto $\mathcal{I}_n^1$, resulting in $N - 1$ vectors in 2-D space, denoted as $\mathbf{z}_2^1, \mathbf{z}_3^1, \cdots, \mathbf{z}_N^1$;

- For these $N - 1$ vectors in 2-D space, solve the LCVBC problem by Algorithm 4 and determine the weight set $\mathcal{W}_1$ for the vertices of the resulting polygon, denoted as $\mathcal{I}_{B,n}^1$;

- For any weight $[w_2^1 \ w_3^1 \ \cdots \ w_N^1] \in \mathcal{W}_1$, the segment $\left\{ \sum_{k=2}^N w_k^1 \mathbf{y}_k + t \cdot \mathbf{y}_1, 0 \leq t \leq 1 \right\}$, parallel to $\mathbf{y}_1$, is an edge of $\mathcal{I}_B$. All the edges of $\mathcal{I}_B$ that are parallel to $\mathbf{y}_1$ can be found in this way due to the following lemma.

Lemma 1. If an edge e of $\mathcal{I}_B$ is parallel to $\mathbf{y}_1$, then the projection of e onto $\mathcal{I}_n^1$ is a vertex of $\mathcal{I}_{B,n}^1$; if v is a vertex of $\mathcal{I}_{B,n}^1$, then $\mathcal{I}_B$ has an edge e such that e is parallel to $\mathbf{y}_1$ and the projection of e onto $\mathcal{I}_n^1$ is v.

Algorithm 5 Linear Combination with Bounded Coefficients: General Cases
---
Input: N vectors in $\mathbb{R}^d$ with $d > 2$: $\mathbf{y}_1, \mathbf{y}_2, \cdots, \mathbf{y}_N$

Output: Vertices and edges of $\mathcal{I}_B$: for each edge, determine its two vertices and their corresponding weights

1: Initialization: $k = 1$;
2: **while** $k \leq N$ **do**
3:        Generate a normal $(d-1)$-plane $\mathcal{I}_n^k$ of $\mathbf{y}_k$;
4:        Project vectors $\mathbf{y}_1, \mathbf{y}_2, \cdots, \mathbf{y}_{k-1}, \mathbf{y}_{k+1}, \cdots, \mathbf{y}_N$ onto $\mathcal{I}_n^k$, resulting $N-1$ vectors in $(d-1)$ space, denoted as $\mathbf{z}_1^k, \mathbf{z}_2^k, \cdots, \mathbf{z}_{k-1}^k, \mathbf{z}_{k+1}^k, \cdots, \mathbf{z}_N^k$;
5:        **if** $d = 3$ **then**
6:             Call Algorithm 4 with input $\mathbf{z}_1^k, \mathbf{z}_2^k, \cdots, \mathbf{z}_{k-1}^k, \mathbf{z}_{k+1}^k, \cdots, \mathbf{z}_N^k$;
7:             Record the weight set $\mathcal{W}_k$ for the vertices of the resulting polygon;
8:        **else**
9:             Call Algorithm 5 with input $\mathbf{z}_1^k, \mathbf{z}_2^k, \cdots, \mathbf{z}_{k-1}^k, \mathbf{z}_{k+1}^k, \cdots, \mathbf{z}_N^k$;
10:            Record the weight set $\mathcal{W}_k$ for the vertices of the resulting polytope;
11:        **end if**
12:        **repeat**
13:             Find $[\, w_1^k \; w_2^k \; \cdots \; w_{k-1}^k \; w_{k+1}^k \; \cdots \; w_N^k \,] \in \mathcal{W}_k$;
14:            Add the following segment to the edge set of $\mathcal{I}_B$

$$\left\{ \sum_{1 \leq j \leq N, j \neq k} w_j^k \mathbf{y}_j + t \cdot \mathbf{y}_k, 0 \leq t \leq 1 \right\}$$

15:            $\mathcal{W}_k \leftarrow \mathcal{W}_k \setminus [\, w_1^k \; w_2^k \; \cdots \; w_{k-1}^k \; w_{k+1}^k \; \cdots \; w_N^k \,]$;
16:        **until** $\mathcal{W}_k = \varnothing$;
17:        $k \leftarrow k + 1$;
18: **end while**

The proof of Lemma 1 is straightforward and omitted for brevity. Fig. 6-3 provides an illustration of the steps above. Following a similar process, one can obtain the edges of $\mathcal{I}_B$ that are parallel to $\mathbf{y}_2, \mathbf{y}_3, \cdots, \mathbf{y}_N$ and in this way, all the edges of $\mathcal{I}_B$ can be determined. Details of the procedure are given in Algorithm 5. One can verify that the computation complexities are $\mathcal{O}(N \log N)$ and $\mathcal{O}(N^{d-1} \log N)$ for Algorithm 4 and Algorithm 5, respectively.

6.3 Optimal Strategy Design

Note that 1) the quest for the optimal strategy of $\mathscr{P}$ can be restricted to the strategies corresponding to the surface of $\mathcal{I}_e$ and 2) the solution for LCVBC problem provides
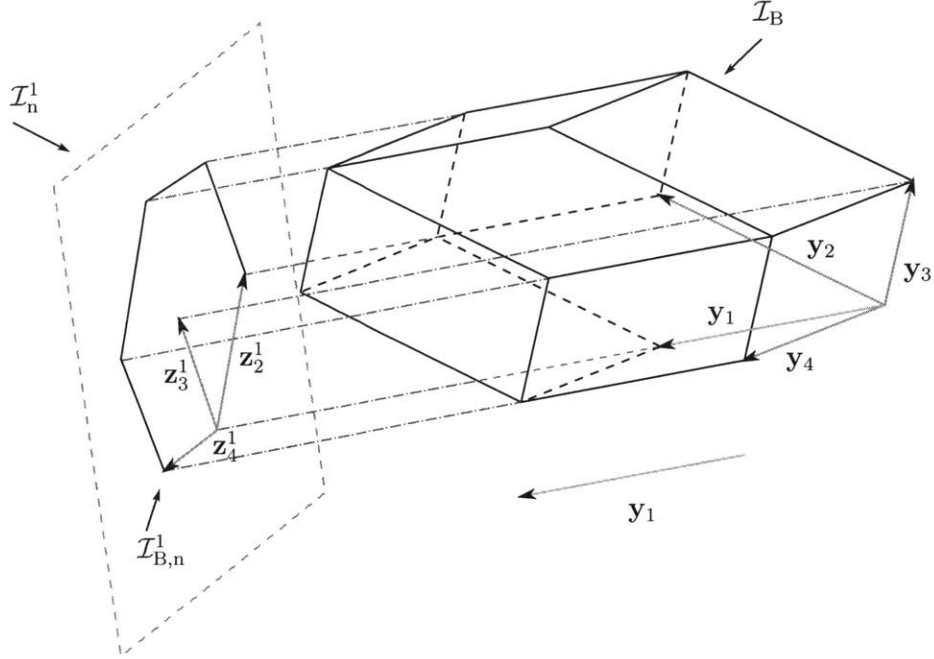
Figure 6-3: Illustration of Linear Combination with Bounded Coefficient in 3-D space: $N = 4$.

an efficient method to determine the triangles on the surface of $\mathcal{I}_e$. These observations lead to Algorithm 6, which gives an optimal resource allocation strategy for $\mathscr{P}$ with individual constraints. The design of Algorithm 6 can be divided into two major parts: Line 2 to Line 5 determine the triangles on the surface of $\mathcal{I}_e$; Line 6 to Line 14 select the strategy corresponding to the triangles on the surface of $\mathcal{I}_e$ with the minimum SPEB. In particular, Line 8 determines the optimal resource allocation strategy corresponding to a triangle on the surface of $\mathcal{I}_e$, which is solved in Chapter 4.1.

Computation complexity of Resource Allocation with Individual Constraints (RAIC): The computation complexity of Line 1 is $\mathcal{O}(n)$. The computation complexity of Line 2 and Line 3 is $\mathcal{O}(n^3 \log n)$ by calling Algorithm 5. Note that $\mathcal{I}_e$ has $\mathcal{O}(n^3)$ edges and $\mathcal{O}(n^3)$ vertices. Hence, the computation complexity for Line 4 and Line 5 are $\mathcal{O}(n^3 \log n)$ and $\mathcal{O}(n^3)$, respectively. Moreover, there are no more than $\mathcal{O}(n^3)$ cycles in the iteration from Line 6 to Line 14 and each cycle can be completed in constant time, implying that the computation complexity of the iteration is $\mathcal{O}(n^3)$. Consequently, the total computation complexity is $\mathcal{O}(n^3 \log n)$.

Algorithm 6 Resource Allocation with Individual Constraints (RAIC)

Input: ξ_k and ϕ_k, $k \in \mathcal{N}_{\mathrm{b}}$; $\mathbf{x}^{\max} \in \mathbb{R}^n$

Output: Optimal RAV $\mathbf{x}^*$ for $\mathscr{P}$

1: Initialization: $\mathcal{P}_{\text{current}}$ is assigned to a sufficiently large number;
2: Call Algorithm 5 with inputs $\mathbf{y}_k = \mathbf{x}_k^{\max} \mathbf{A}_{\mathrm{c}} \, \mathbf{e}_k$, $k \in \mathcal{N}_{\mathrm{b}}$, and translate the resulting polytope by $\mathbf{b}_{\mathrm{e}}$, providing $\mathcal{X}_{\mathrm{F}}$;
3: Intersect $\mathcal{X}_{\mathrm{F}}$ with $\mathcal{I}_{\mathrm{F}}$ and project the results onto $\mathbb{R}^3$ to obtain the vertices of $\mathcal{I}_{\mathrm{e}}$;
4: Generate the convex hull for the vertices of $\mathcal{I}_{\mathrm{e}}$;
5: Find a triangulation for the faces of $\mathcal{I}_{\mathrm{e}}$ and let $\mathcal{K}$ denote the set consisted of all the resulting triangles;
6: **repeat**
7:     Find an element $K_i \in \mathcal{K}$;
8:     Find the optimal RAV $\widetilde{\mathbf{x}}$ corresponding to K_i based on the solution for $\mathscr{P}_{\mathrm{S}}$;
9:     **if** $\mathcal{P}(\widetilde{\mathbf{x}}) \leq \mathcal{P}_{\text{current}}$ **then**
10:         $\mathcal{P}_{\text{current}} \leftarrow \mathcal{P}(\widetilde{\mathbf{x}})$;
11:         $\mathbf{x}^* \leftarrow \widetilde{\mathbf{x}}$;
12:     **end if**
13:     $\mathcal{K} \leftarrow \mathcal{K} \setminus \{K_i\}$;
14: **until** $\mathcal{K} = \varnothing$
15: Output $\mathbf{x}^*$.

Chapter 7

Discussions

This chapter presents the discussions on several related issues: (1) robust formulation; (2) exact SPEB expression with prior knowledge; and (3) efficient resource allocation algorithms.

7.1 Robust Formulation

The design of resource allocation strategies is determined by the network parameters, which cannot always be perfectly estimated. These estimated values are subject to uncertainties, and the use of estimated values may result in suboptimal solutions. Hence, it is necessary to construct robust formulations accounting for the parameter uncertainties. Let $\xi_k \in \mathcal{S}_k^\xi$ and $\phi_k \in \mathcal{S}_k^\phi$, where

$$\mathcal{S}_k^\xi := \left[\hat{\xi}_k - \epsilon_k^\xi, \, \hat{\xi}_k - \epsilon_k^\xi \right] = \left[\underline{\xi}_k, \, \overline{\xi}_k \right]$$

$$\mathcal{S}_k^\phi := \left[\hat{\phi}_k - \epsilon_k^\phi, \, \hat{\phi}_k - \epsilon_k^\phi \right] = \left[\underline{\phi}_k, \, \overline{\phi}_k \right]$$

in which $\hat{\xi}_k$ and $\hat{\phi}_k$ denote the nominal values of the ERC and angles and ϵ_k^ξ and ϵ_k^ϕ denote ERC and angle uncertainties. In this setting, the worst-case SPEB is given by

$$\mathcal{P}_{\mathrm{R}}(\mathbf{x}) = \max_{\xi_k \in \mathcal{S}_k^\xi, \phi_k \in \mathcal{S}_k^\phi} \mathcal{P}(\mathbf{x}) = \max_{\xi_k = \underline{\xi}_k, \phi_k \in \mathcal{S}_k^\phi} \mathcal{P}(\mathbf{x})$$

where the second equation is due to the fact that the SPEB monotonically decreases in ξ_k.[1]

Direct maximization over ϕ_k is non-trivial. To address this problem, an auxiliary matrix is introduced as

$$\mathbf{Q}_{\mathrm{e}}(\mathbf{p}_0; \mathbf{x}) = \mathbf{J}_0 + \sum_{k \in \mathcal{N}_{\mathrm{b}}} \underline{\xi}_k x_k \cdot (\mathbf{J}_{\mathrm{r}}(\hat{\phi}_k) - \delta_k \cdot \mathbf{I})$$

where $\delta_k = \sin \epsilon_k^\phi$. It has been shown in [37] that for any $\phi_k \in \mathcal{S}_k^\phi$, $\xi_k \in \mathcal{S}_k^\xi$,

$$\mathbf{Q}_{\mathrm{e}}(\mathbf{p}_0; \mathbf{x}) \preceq \mathbf{J}_{\mathrm{e}}(\mathbf{p}_0; \mathbf{x})$$

and concequently,

$$\overline{\mathcal{P}}_{\mathrm{R}}(\mathbf{x}) := \mathrm{tr}\{\mathbf{Q}_{\mathrm{e}}^{-1}(\mathbf{p}_0; \mathbf{x})\} \geq \mathrm{tr}\{\mathbf{J}_{\mathrm{e}}^{-1}(\mathbf{p}_0; \mathbf{x}) = \mathcal{P}(\mathbf{x})$$

provided that $\mathbf{Q}_{\mathrm{e}}(\mathbf{p}_0; \mathbf{x}) \succeq 0$. With this observation, the robust resource allocation problem, denoted as $\overline{\mathscr{P}}_{\mathrm{R}}$, can be formulated as minimizing $\overline{\mathcal{P}}_{\mathrm{R}}(\mathbf{x})$ subject to resource constraints.

Consider an affine transformation

$$\mathbf{y} = \hat{\mathbf{A}}\mathbf{x} + \mathbf{b}$$

where $\hat{\mathbf{A}} = [\,\mathbf{c} \ \ \mathbf{s} \ \ \mathbf{1} - 2\boldsymbol{\delta}\,]^{\mathrm{T}} \underline{\mathbf{R}}$, in which $\boldsymbol{\delta} = [\,\delta_1 \, \delta_2 \, \cdots \, \delta_n\,]^{\mathrm{T}}$ and $\underline{\mathbf{R}} = \mathrm{diag}\{\underline{\xi}_1, \underline{\xi}_2, \cdots, \underline{\xi}_n\}$. With this transformation, the geometric methods proposed in Chapter 3 to Chapter 6 can be used to solve the robust resource allocation problem $\overline{\mathscr{P}}_{\mathrm{R}}$.

7.2   Exact SPEB with Prior Knowledge

We next show that the geometric methods developed in this chapter can be used to solve resource allocation problems that adopt the exact SPEB as the performance

---

[1]The monotonicity of SPEB in RC can be proved similarly to Proposition 2.

metric.

The exact EFIM is given by [7]

$$\bar{\mathbf{J}}_{\mathrm{e}}(\mathbf{p}_0; \mathbf{x}) = \mathbf{J}_0 + \sum_{k \in \mathcal{N}_{\mathrm{b}}} x_k \mathbf{J}_k$$

where $\mathbf{J}_k = \mathbb{E}\{\xi_k \mathbf{J}_{\mathrm{r}}(\phi_k)\}$, in which the expectation is with respect to the distributions of the agent's prior positional knowledge, the prior RC knowledge, and the observation noise. Consequently, the exact expression of the SPEB is

$$\mathcal{P}(\mathbf{x}) = \mathrm{tr}\left\{\bar{\mathbf{J}}_{\mathrm{e}}^{-1}(\mathbf{p}_0; \mathbf{x})\right\}.$$

Note that by eigenvalue decomposition, the EFIM $\mathbf{J}_k$ can be decomposed as

$$\mathbf{J}_k = \xi_k^{(1)} \mathbf{J}_{\mathrm{r}}(\varphi_k) + \xi_k^{(2)} \mathbf{J}_{\mathrm{r}}(\varphi_k + \pi/2)$$

where $\xi_k^{(1)}, \xi_k^{(2)} \geq 0$ are the eigenvalues of $\mathbf{J}_k$ and φ_k, $\varphi_k + \pi/2$ are the angles of the corresponding eigenvectors. Consider an affine transformation

$$\mathbf{y} = \bar{\mathbf{A}}\,\mathbf{x} + \mathbf{b}$$

where

$$\bar{\mathbf{A}} = [\,\widetilde{\mathbf{c}}\ \ \widetilde{\mathbf{s}}\ \ 1\,]^{\mathrm{T}}\,\mathbf{R}^{(1)} - [\,\widetilde{\mathbf{c}}\ \ \widetilde{\mathbf{s}}\ \ -1\,]^{\mathrm{T}}\,\mathbf{R}^{(2)}$$

in which

$$\mathbf{R}^{(i)} = \mathrm{diag}\{\xi_1^{(i)}, \xi_2^{(i)}, \cdots, \xi_n^{(i)}\}, \ \ i = 1, 2$$

and

$$\widetilde{\mathbf{c}} = [\,\cos 2\varphi_1\ \ \cos 2\varphi_2\ \ \cdots\ \ \cos 2\varphi_n\,]^{\mathrm{T}}$$

$$\widetilde{\mathbf{s}} = [\,\sin 2\varphi_1\ \ \sin 2\varphi_2\ \ \cdots\ \ \sin 2\varphi_n\,]^{\mathrm{T}}.$$

With this transformation, the methods proposed in Chapter 3 to Chapter 6 can be used to solve the resource allocation problem with the exact EFIM. Note that computing the exact SPEB involves the integration over the distribution of the agent's prior knowledge. Hence, the approximated SPEB is more favorable to be used as the performance metric.

7.3 Heuristic Resource Allocation Strategies

We next propose some heuristic resource allocation strategies in WNL. The performance of these strategies will be evaluated in Chapter 8.

7.3.1 No Individual Constraints

The following three strategies are proposed to solve $\mathscr{P}$ without individual constraints (2.5).

- Uniform strategy: allocate transmit resources equally among anchors;

- Strategy I: select three anchors corresponding to the largest RCs; find the optimal RAV for this simple network;

- Strategy II: divide the anchors $k \in \mathcal{N}_b$ into three groups $\mathcal{G}_1$, $\mathcal{G}_2$, and $\mathcal{G}_3$: $k \in \mathcal{G}_1$ if $\phi_k \in [0, 2\pi/3)$; $k \in \mathcal{G}_2$ if $\phi_k \in [2\pi/3, 4\pi/3)$; and $k \in \mathcal{G}_3$ if $\phi_k \in [4\pi/3, 2\pi)$; select the anchor with the maximum RC in each group; find the optimal RAV for this simple network;

- Strategy III: search all $\binom{n}{3}$ simple networks and select the one with the minimum SPEB, proposed in Chapter 4.3.

7.3.2 With Individual Constraints

The following strategies are proposed to solve $\mathscr{P}$ with individual constraints (2.5).

52

Algorithm 7 Strategy IV and V
___
Input: ξ_k and ϕ_k, $k \in \mathcal{N}_\mathrm{b}$; $\mathbf{x}^\mathrm{max} \in \mathbb{R}^n$
Output: An RAV $\mathbf{x}$ for $\mathscr{P}$ with (2.5)
 1: $\overline{\mathcal{U}} \leftarrow \varnothing$;
 2: **repeat**
 3:     Determine a solution $\mathbf{x}$ of $\mathscr{P}_\mathrm{M}$ for given $\overline{\mathcal{U}}$ (either adopting RAIV or Uniform Strategy);
 4:     **for** $k \in \mathcal{N}_\mathrm{b} \setminus \overline{\mathcal{U}}$ **do**
 5:         **if** $x_k > \underline{\mathbf{x}_k^\mathrm{max}}$ **then**
 6:             $\overline{\mathcal{U}} \leftarrow \overline{\mathcal{U}} \cup \{k\}$;
 7:         **end if**
 8:     **end for**
 9: **until** $\mathbf{x} \preceq \mathbf{x}_k^\mathrm{max}$
10: Output $\mathbf{x}$.
___

Strategy IV operates in an iterative way and it maintains an *upper bound anchor set* $\overline{\mathcal{U}}$, which records the indexes of anchors that do not satisfy the individual constraints (2.5) in the iterations. Details are given in Algorithm 7. Note that in Line 3, Strategy IV adopts RAIV to solve problem $\mathscr{P}_\mathrm{M}$.

$$\mathscr{P}_\mathrm{M}: \qquad \min_{\{\mathbf{x}\}} \quad \mathcal{P}(\mathbf{x})$$

$$\mathrm{s.t.} \quad \mathbf{1}^\mathrm{T}\mathbf{x} \leq 1$$

$$x_k = \mathbf{x}_k^\mathrm{max}, \quad k \in \overline{\mathcal{U}}$$

$$\mathbf{x} \succeq \mathbf{0}.$$

Strategy V follows the same procedure as Strategy IV except that Strategy V adopts Uniform Strategy to solve $\mathscr{P}_\mathrm{M}$ in Line 3. Note that there are no more than n cycles in the iteration from Line 4 to Line 9. Hence, the computation complexities are $\mathcal{O}(n^2 \log n)$ and $\mathcal{O}(n^2)$ for Strategy IV and V, respectively.

Strategy VI first finds the triangles on the surface of $\mathcal{I}_\mathrm{e}$ by determining $\mathcal{E}_\mathrm{I}$ and $\mathcal{I}_\mathrm{e} = \mathcal{CH}\{\mathcal{E}_\mathrm{I}\}$ and then follows Line 6 to 15 in Algorithm 6 to provide an optimal RAV. One can verify that the complexity of Strategy VI is $\mathcal{O}(n2^n)$.

The computation complexities of all the proposed strategies are given in Table I.

Table 7.1: Computation complexity for strategies with and without individual constraints

	Optimal		Suboptimal	
	Name	Time	Name	Time
$\mathscr{P}$ without (2.5)	RAGM	$\mathcal{O}(n \log n)$	Uniform	$\mathcal{O}(1)$
	RAIV	$\mathcal{O}(n \log h)$	Stra. II	$\mathcal{O}(n)$
	Stra. III	$\mathcal{O}(n^3)$	Stra. I	$\mathcal{O}(n)$
$\mathscr{P}$ with (2.5)	RAIC	$\mathcal{O}(n^3 \log n)$	Stra. IV	$\mathcal{O}(n^2 \log n)$
	Stra. VI	$\mathcal{O}(n2^n)$	Stra. V	$\mathcal{O}(n^2)$

Chapter 8

Numerical Results

This chapter provides numerical results to illustrate the sparsity of optimal resource allocation and to evaluate the performance of the proposed strategies.

8.1 Anchor Selection for a Simple Network

First consider an example of anchor selection where the agent is located at different positions. Three anchors (A, B and C) are deployed at the vertices of an equilateral triangle. Consider the RC $\zeta_k = \xi_k d_k^2$ and $\zeta_k = 100$. The plane is divided into four types of regions labeled as I, II, III, and IV (see Fig. 8-1). The resource allocation strategy that achieves the optimal localization performance requires different sets of anchors corresponding to the agent's position. For instance, the resources are allocated to all the three anchors if the agent is in region IV. First, the area of region IV is relatively small, implying that in most cases only two anchors are required to achieve the optimal localization performance. Second, if the agent is in the "far field" region, i.e., it is sufficiently far away from all the anchors, the optimal strategy for $\mathscr{P}$ requires two active anchors. Third, if the agent lies on the line formed by two anchors, only the anchor closer to the agent is used to achieve the optimal localization performance. This is intuitive since allocating resources to the closer anchor is more efficient for improving the localization performance.
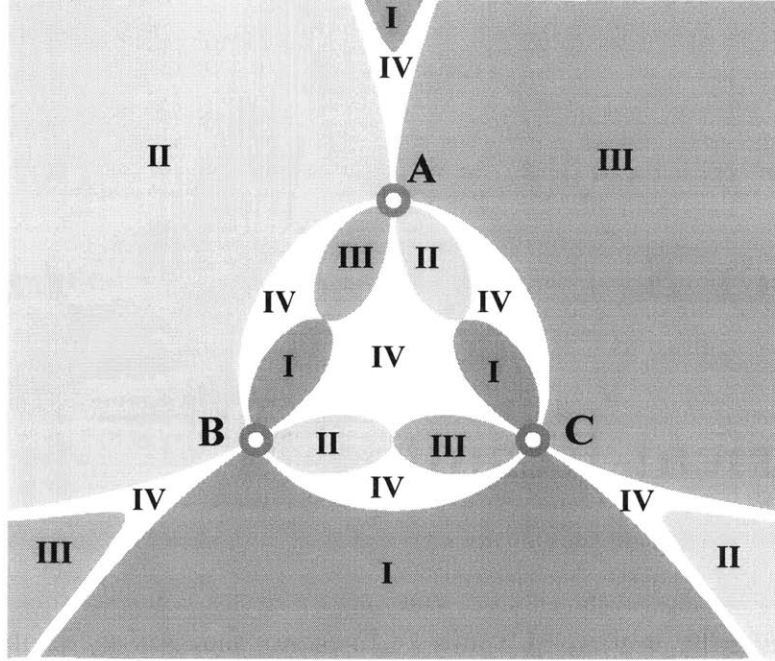
Figure 8-1: The optimal strategy for $\mathscr{P}$ uses B and C if the agent is in region I; it uses A and B if the agent is in region II; it uses A and C if the agent is in region III; and it uses A, B and C if the agent is in region IV.

8.2 Performance of Resource Allocation Strategies

Consider a 2-D network where an agent and anchors are placed randomly in the square region (10m × 10m) with uniform distribution. Consider that the RCs $\{\zeta_k\}_{k \in \mathcal{N}_b}$ are modeled as independent Rayleigh random variables with mean 100.

Case 1) No Prior Knowledge, No Individual Constraints: The performance of the optimal strategy and three other efficient strategies (i.e., the Uniform strategy, Strategy I and Strategy II) are compared. Fig. 8-2 shows the SPEB as a function of the number of anchors for different strategies. First, the achieved SPEB decreases with the number of anchors for each strategy since more anchors provide more degrees of freedom, resulting in higher diversity gain. Second, the optimal strategy outperforms all the heuristic algorithms, e.g., reducing the SPEB by more than 50%, 40%, and 20% compared to Uniform strategy, Strategy I and Strategy II, respectively, when $n = 10$. Third, Strategy II outperforms Strategy I, and they both perform better than Uniform strategy. This agrees with intuition because Strategy II accounts for

Figure 8-2: Average SPEB as a function of the number of anchors for the optimal strategy, Strategy I, Strategy II, and the Uniform strategy without prior positional knowledge.

the effects of both angles and ERCs while Strategy I considers only ERCs.

Case 2) Prior Knowledge, No Individual Constraints: The performances of the optimal strategy and three efficient strategies (i.e., Uniform strategy, Strategy I and Strategy II) are compared. The prior positional knowledge of the agent follows a Gaussian distribution $\mathcal{N}(\mathbf{p}_0, \sigma^2 \mathbf{I}_2)$, where $\mathbf{p}_0 = [\, 0 \; 0\,]^{\mathrm{T}}$ and σ is the standard deviation of the prior position distribution. Fig. 8-3 shows the SPEB as a function of the number of anchors for different strategies with $\sigma^2 = 10$ and $\sigma^2 = 1$. First, it can be observed that the SPEB decreases with the number of anchors for all strategies due to the diversity gain. Second, the optimal strategy, Strategy I, and Strategy II all outperform Uniform strategy significantly, e.g., reducing the SPEB by more than 30% when $n = 10$. Third, the SPEB increases with the variance σ^2 of the prior knowledge. Moreover, the SPEB values of Strategy I and II are closer to that of the optimal strategy when σ^2 is smaller. This is because smaller variance σ^2 translates into more prior positional knowledge and thus, ranging measurements contribute less
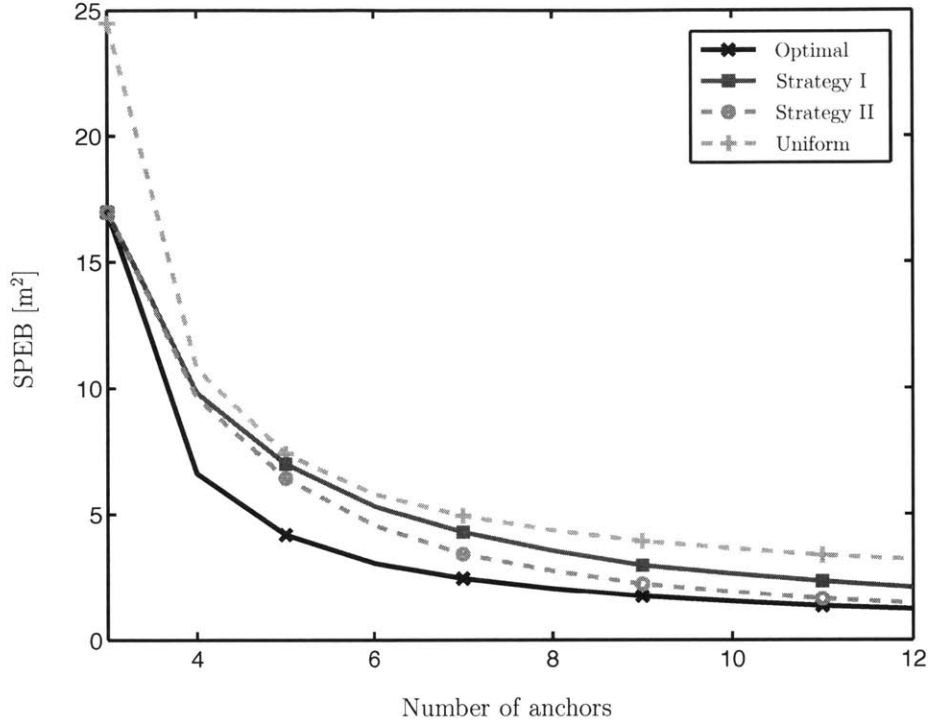
57
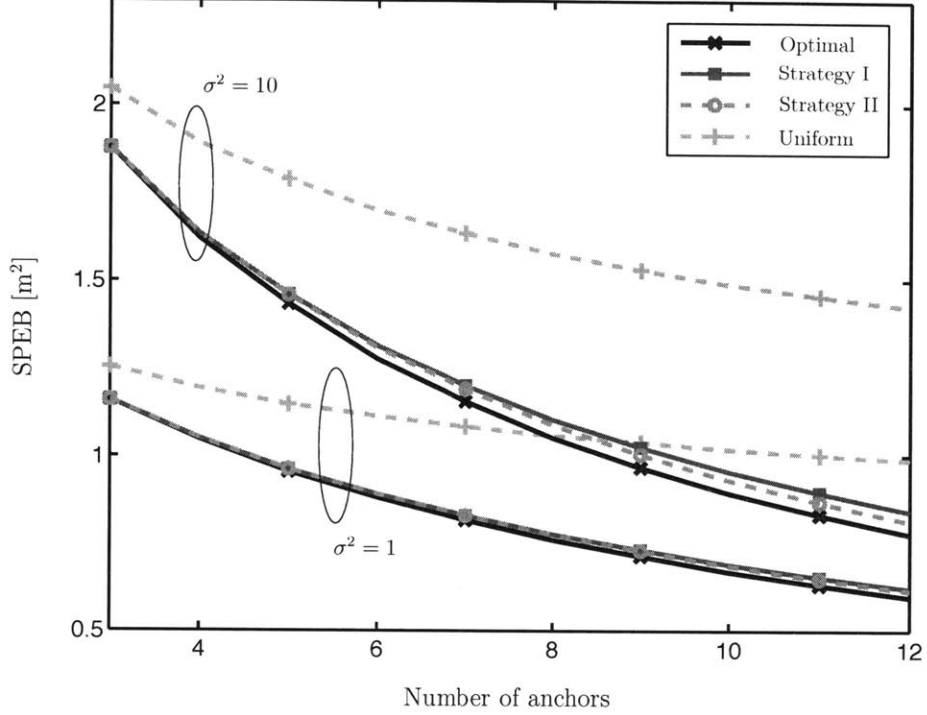
Figure 8-3: Average SPEB as a function of the number of anchors for the optimal strategy, Strategy I, Strategy II and Uniform strategy with prior positional knowledge.

to the localization performance.

Case 3) Individual Resource Constraints: The performance of the optimal strategy, Strategy IV, and Strategy V are compared.

Consider that the upper bound of the individual resource follows an i.i.d. uniform distribution over different anchors, i.e., $\mathbf{x}_k^{\max} \sim \mathrm{U}(0, \overline{P})$, $\forall k \in \mathcal{N}_{\mathrm{b}}$, where $\overline{P}$ is a parameter to be selected. Fig. 8-4 shows the SPEB as a function of the number of anchors for different strategies with $\overline{P} = 0.2$ and 1. First, the SPEB decreases with the number of anchors due to the diversity gain. Second, Strategy IV and the optimal strategy provide almost the identical performance, significantly outperforming Strategy V, e.g., reducing the SPEB by more than 40% when $n = 10$. Third, the SPEB decreases with $\overline{P}$ for the optimal strategy and Strategy IV because smaller $\overline{P}$ implies smaller feasible set for the optimal strategy and Strategy IV, and therefore leads to larger SPEB. Fourth, the SPEB achieved by Strategy V has almost the same value for $\overline{P} = 0.2$ and 1. This is because Strategy V usually allocates the resources evenly
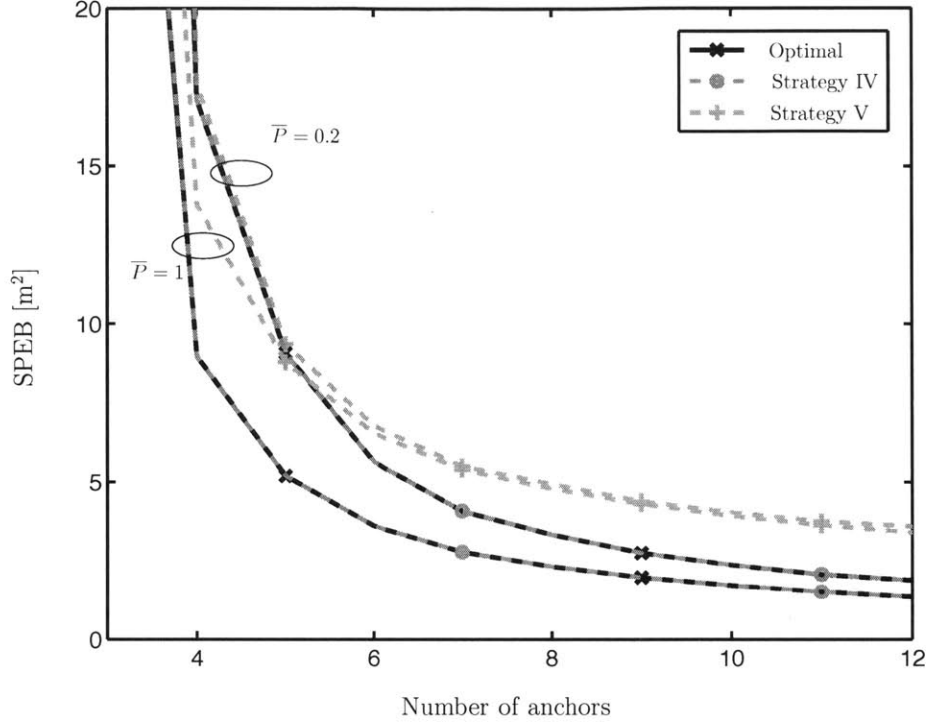
Figure 8-4: Average SPEB as a function of the number of anchors for the optimal strategy, Strategy IV and Strategy V.

among anchors and hence individual resource constraints are often inactive, leading to the fact that Strategy V provides almost the same performance for different $\overline{P}$.

Now consider that the upper bound of the individual resource is a constant for different anchors, i.e., $\mathbf{x}_{\max}^k = \overline{P}, \forall k$. Fig. 8-5 shows the SPEB as a function of $\overline{P}$ for different strategies with $n = 10$ and 20. First, the SPEB decreases with $\overline{P}$ for both Strategy IV and the optimal strategy because larger $\overline{P}$ implies more relaxed individual constraints. This decreasing trend vanishes as $\overline{P}$ increases because the individual constraints are inactive for large $\overline{P}$. Second, it can be observed that Strategy V provides almost the same SPEB for different $\overline{P}$, similarly to Fig. 8-4. Third, Strategy IV and the optimal strategy provide almost the identical performance, outperforming Strategy V significantly. Fourth, the SPEB for $n = 20$ is less than that for $n = 10$ due to the diversity gain.

59
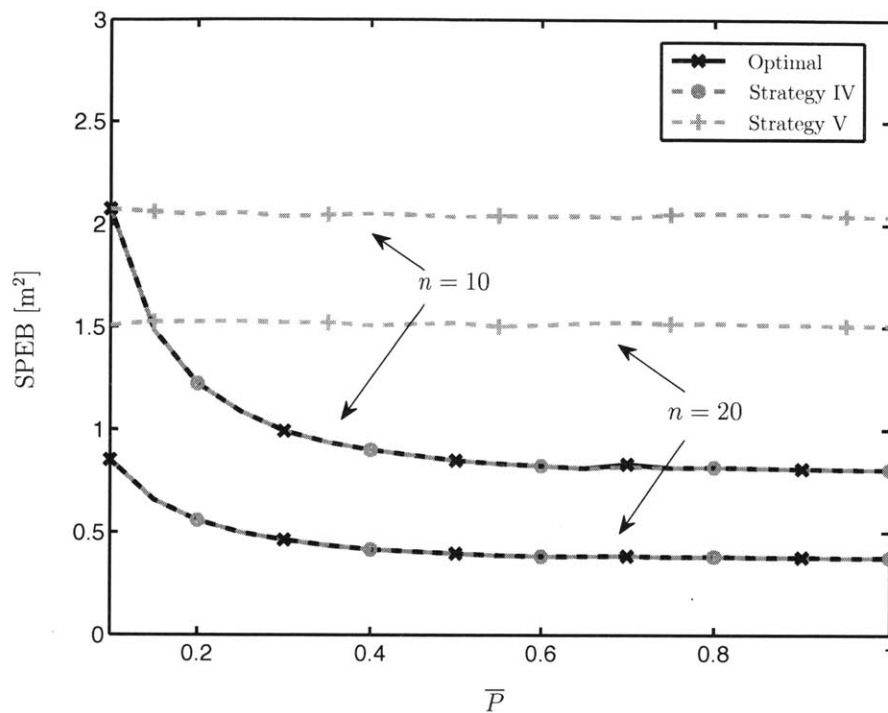
Figure 8-5: Average SPEB as a function of $\overline{P}$ for the optimal strategy, Strategy IV and Strategy V.

8.3 Efficiency of Geometric Methods

The efficiency of the proposed strategies is compared in this section under the same network setting as Chapter 8.2. The proposed strategies are run on a 2-GHz personal computer.

Case 1) No Individual Constraints: Fig. 8-6 shows the running time as a function of the number of anchors for Strategy III, RAGM, and RAIV. First, the running time increases with the number of anchors and the increasing speed differs for different strategies. This agrees with the computation complexity analysis in Chapter 4.3 and Chapter 5. Second, in terms of the running time, RAIV outperforms RAGM, and they both outperform Strategy III significantly, especially when n is large. Third, the running time for RAIV almost remains a constant as n increases. This is because the running time of RAIV consists of two terms: $\mathcal{O}(n \log h)$ for generating the convex hull and $\mathcal{O}(h)$ for searching the set $\widetilde{\mathcal{K}}$. When n is small, the second term dominates
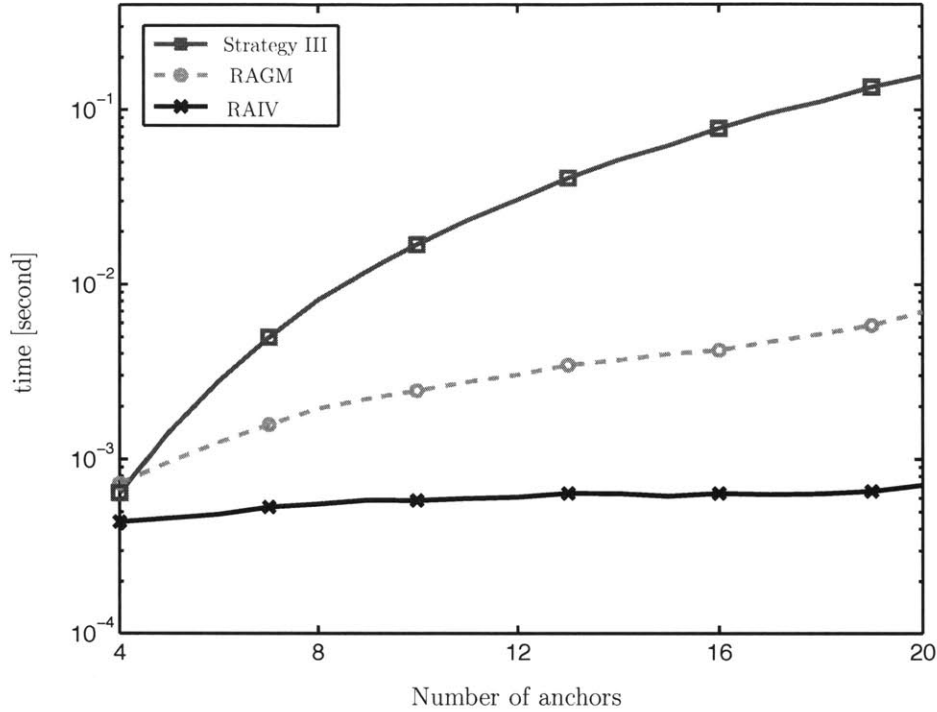
Figure 8-6: Running time as a function of the number of anchors for Strategy III, RAGM and RAIV.

the running time. Since h remains almost the same when n is small, as shown in Fig. 5-2, the running time for the second term does not increase and hence the total running time is almost a constant.

Case 2) Individual Resource Constraints: Fig. 8-7 shows the running time as a function of the number of anchors for RAIC, Strategy IV, and Strategy VI. First, Strategy IV and RAIC outperform Strategy VI significantly in the running time, e.g., reduce the running time by more than 98% when $n = 15$. Second, the running time gap between Strategy VI and the other two strategies increases with the number of anchors. The linearity of the curve for Strategy VI shows that the computation complexity grows exponentially with n, which agrees with the analysis in Chapter 6.1 and shows that Strategy VI is impractical to implement. Third, Strategy IV has much less running time than the optimal strategy RAIC. Considering its near-optimal performance shown in Figs. 8-4 and 8-5, Strategy IV achieves a good tradeoff between performance and complexity.
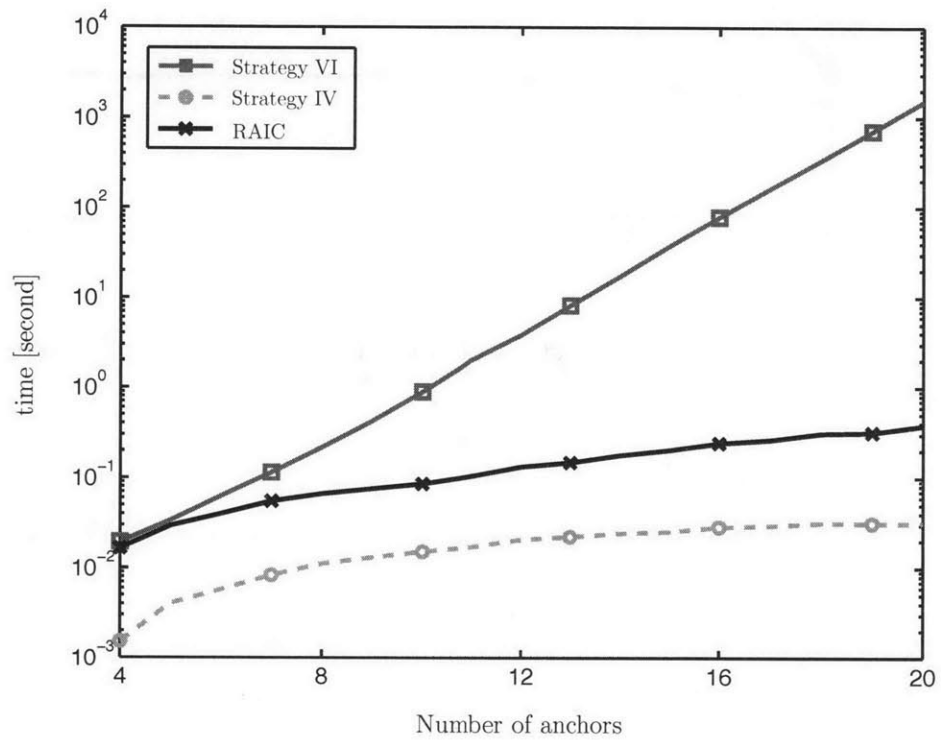
Figure 8-7: Running time as a function of the number of anchors for Strategy VI, Strategy IV and RAIC.

Chapter 9

Conclusion

In this thesis, we established a computational geometry framework for efficient resource allocation in WNL. The proposed approach used the low-dimensionality property of the localization performance metric. By mapping a resource allocation strategy into a point in 3-D Euclidian space, we obtained the geometric interpretation of the RAV and the SPEB, and then developed important geometric properties of the optimal RAV. These properties enabled us not only to reveal the sparsity property of the optimal RAV, but also to design efficient resource allocation strategies. The proposed strategies, with complexity $\mathcal{O}(n \log n)$, are more efficient than SDP and SOCP-based approaches. For resource allocation problems with individual constraints, we proposed a dimension augmentation and projection method that coped with the high computation complexity brought by the individual constraints. The proposed strategy, with complexity $\mathcal{O}(n^3 \log n)$, is much more efficient than an exhaustive search with an exponential complexity of $\mathcal{O}(2^n)$. The performance of different resource allocation strategies was compared in the simulation results. It was demonstrated that the optimal resource allocation strategies obtained via the geometric methods significantly outperformed most heuristic strategies. Our results provide a new methodology for resource allocation design in network localization as well as insights into the optimization problems with similar structures.

Appendix A

Appendices

A.1 Application of the Resource Allocation Problems

The EFIM is given by [7]

$$\mathbf{J}_e = \mathbf{J}_0 + \sum_{k \in \mathcal{N}_b} \varrho_k \, p_k \left(\int_{-\infty}^{+\infty} f^2 |S_k(f)|^2 df \right) \mathbf{J}_r(\phi_k)$$

in which

$$\varrho_k = \frac{8\pi^2 |\alpha_k^{(1)}|^2 (1 - \chi_k)}{N_0 c_{tr}^2 \, d_k^{2\beta}}$$

with $S_k(f)$ denoting the Fourier transform of $s_k(t)$ and $\chi_k \in [0, 1]$ denoting the path-overlap coefficient. Next we show that power allocation and bandwidth allocation problems in WNL can be converted to $\mathscr{P}$.

Power Allocation

The power allocation problem for WNL is equivalent to $\mathscr{P}$ with $x_k = p_k$ and

$$\xi_k = \varrho_k \int_{-\infty}^{+\infty} f^2 |S_k(f)|^2 df.$$

Bandwidth Allocation

For a given aggregate signal $S(f)$ in frequency domain, determining a n-partition of the support of $S(f)$ is to find $\mathcal{F}_k(k \in \mathcal{N}_b)$, so that $\cup_{k \in \mathcal{N}_b} \mathcal{F}_k = \{f : S(f) \neq 0\}$ and $\mathcal{F}_k \cap \mathcal{F}_j = \emptyset$, $1 \le k \neq j \le n$. The bandwidth allocation problem is to find the n-partition of a given aggregate signal $S(f)$ so that the corresponding SPEB is minimized. Hence, the bandwidth allocation problem is equivalent to $\mathscr{P}$ with

$$x_k = \frac{\int_{\mathcal{F}_k} f^2 |S(f)|^2 df}{\int_{-\infty}^{+\infty} f^2 |S(f)|^2 df}$$

and $\xi_k = \varrho_k p_k$.

A.2 Proof of Theorem 2

The following lemma will be used in the proof.

Lemma 2. Given $n \in \mathbb{N}$ and $\mathbf{y}, \mathbf{z} \in \mathbb{R}^n$, if $\mathbf{y} \succ \mathbf{0}$ and $\mathbf{z} \neq \mathbf{0}$, there exists $\tilde{t} \in \mathbb{R}$ such that $\mathbf{y} + \tilde{t}\mathbf{z} \succeq \mathbf{0}$ and $\|\mathbf{y} + \tilde{t}\mathbf{z}\|_0 < n$.

Proof. This lemma can be proved by considering a mapping $f : \mathbb{R} \to \mathbb{R}^n$

$$f(t) = \mathbf{y} + t\,\mathbf{z}.$$

Note that (i) $f(0) = \mathbf{y}$ is a vector with all positive elements; (ii) for sufficiently large M, if $t > M$, then either $f(t)$ or $f(-t)$ has at least one negative element; (iii) $f(\cdot)$ is continuous on t. Thus, there exists $\tilde{t}$ such that $f(\tilde{t}) \succeq \mathbf{0}$ with $f(\tilde{t})$ containing at least one zero element, i.e., $\|f(\tilde{t})\|_0 < n$. $\qquad\square$

Let $\mathbf{x}^*$ denote an optimal RAV for $\mathscr{P}$ with the minimum number of positive elements and let $m = \|\mathbf{x}^*\|_0$. If $m \le M$, the proof is completed. We next show that $m > M$ will lead to contradiction.

Without loss of generality, consider that the first m elements of $\mathbf{x}^*$ are positive,

i.e.,

$$\mathbf{x}^* = [\,\mathbf{x}^\mathrm{T} \quad \mathbf{0}_{M-m}^\mathrm{T}\,]^\mathrm{T}.$$

Let $\mathbf{Q}(\mathbf{y})$ denote a function of $\mathbf{y} \in \mathbb{R}^m$

$$\mathbf{Q}(\mathbf{y}) = \mathbf{J}_0 + \sum_{k=1}^{m} y_k\,\mathbf{C}_k$$

where $\mathbf{C}_k = \xi_k \mathbf{u}_k\,\mathbf{u}_k^\mathrm{T}$ is a symmetric $d \times d$ matrix. Then $\mathbf{J}_e(\mathbf{p}_0; \mathbf{x}^*)$ can be written as

$$\mathbf{J}_e(\mathbf{p}_0; \mathbf{x}^*) = \mathbf{J}_0 + \sum_{k=1}^{m} x_k^* \mathbf{C}_k = \mathbf{Q}(\mathbf{x})$$

Let $[\mathbf{C}_k]_{ij} = c_k^l$ denote the elements of $\mathbf{C}_k$, where $l = \binom{j}{2} + i$. Let $\mathbf{c}_l = [\,c_1^l \;\; c_2^l \;\; \cdots \;\; c_m^l\,]^\mathrm{T}$ for $l = 1, 2, \cdots, M$. The elements of $\mathbf{Q}(\mathbf{x})$ can then be written as

$$
\begin{aligned}
[\,\mathbf{Q}(\mathbf{x})\,]_{ij} &= [\mathbf{J}_0]_{ij} + \sum_{k=1}^{m} x_k^* \,[\mathbf{C}_k]_{ij} \\
&= [\mathbf{J}_0]_{ij} + \mathbf{x}^\mathrm{T}\,\mathbf{c}_l.
\end{aligned}
\tag{A.1}
$$

Since $\mathbf{c}_l \in \mathbb{R}^m$ and $m > M$, there exists a vector $\mathbf{g} \in \mathbb{R}^m$ orthogonal to $\{\,\mathbf{c}_l : l = 1, 2, \cdots, M\,\}$. Hence, for any $\eta \in \mathbb{R}$, $1 \le i, j \le d$,

$$[\,\mathbf{Q}(\mathbf{x} + \eta\,\mathbf{g})\,]_{ij} = [\mathbf{J}_0]_{ij} + (\mathbf{x} + \eta\,\mathbf{g})^\mathrm{T}\,\mathbf{c}_l = [\mathbf{Q}(\mathbf{x})]_{ij}$$

where the last equation is due to (A.1). This shows the invariance of EFIM with respect to RAV in the direction of $\mathbf{g}$. Next we show the contradiction for both cases $\mathbf{g}^\mathrm{T}\mathbf{1} \neq 0$ and $\mathbf{g}^\mathrm{T}\mathbf{1} = 0$, respectively.

If $\mathbf{g}^\mathrm{T}\mathbf{1} \neq 0$, choose ϵ such that 1) $\epsilon \cdot \mathbf{g}^\mathrm{T}\mathbf{1} < 0$ and 2) $\mathbf{x} + \epsilon\,\mathbf{g} \succeq \mathbf{0}$.[1] Let $\tilde{\mathbf{x}} = \mathbf{x} + \epsilon\,\mathbf{g}$ and $\tilde{\mathbf{x}}^* = [\,\tilde{\mathbf{x}}^\mathrm{T} \quad \mathbf{0}_{M-m}^\mathrm{T}\,]^\mathrm{T}$. Then

$$\mathbf{1}_n^\mathrm{T}\tilde{\mathbf{x}}^* = \mathbf{1}_m^\mathrm{T}\tilde{\mathbf{x}} < \mathbf{1}_m^\mathrm{T}\mathbf{x} = \mathbf{1}_n^\mathrm{T}\mathbf{x}^*.$$

---

[1]This is achievable since $\mathbf{x} \succ \mathbf{0}$, one can choose ϵ with $|\epsilon|$ sufficiently small.

Choose $\mathbf{y} = (\mathbf{1}_n^T \mathbf{x}^* / \mathbf{1}_n^T \tilde{\mathbf{x}}^*) \cdot \tilde{\mathbf{x}}^*$. One can verify that

$$\mathcal{P}(\mathbf{y}) \overset{(a)}{<} \mathcal{P}(\tilde{\mathbf{x}}^*) = \mathcal{P}(\mathbf{x}^*). \tag{A.2}$$

where (a) is due to the fact that $\mathbf{J}_e(\mathbf{p}_0; \mathbf{y}) \succ \mathbf{J}_e(\mathbf{p}_0; \tilde{\mathbf{x}}^*)$. Equation (A.2) implies that $\mathbf{y}$ outperforms $\mathbf{x}^*$, which contradicts the assumption that $\mathbf{x}^*$ is an optimal solution for $\mathcal{P}$.

If $\mathbf{g}^T \mathbf{1} = 0$, consider $h(\eta) = \mathbf{x} + \eta \mathbf{g}$. By Lemma 2, there exists η_1 such that $h(\eta_1) \succeq \mathbf{0}$ and $\|h(\eta_1)\|_0 < m$. Let $\mathbf{x}' = h(\eta_1)$ and $\mathbf{x}'^* = [\mathbf{x}'^T \ \mathbf{0}_{M-m}^T]^T$. Note that (1) $\|\mathbf{x}'^*\|_0 = \|h(\eta_1)\|_0 < m = \|\mathbf{x}^*\|_0$; (2) $\mathbf{J}_e(\mathbf{p}_0; \mathbf{x}'^*) = \mathbf{Q}(\mathbf{x} + \eta_1 \mathbf{g}) = \mathbf{Q}(\mathbf{x}) = \mathbf{J}_e(\mathbf{p}_0; \mathbf{x}^*)$ and hence $\mathcal{P}(\mathbf{x}'^*) = \mathcal{P}(\mathbf{x}^*)$; and (3) $\mathbf{1}^T \mathbf{x}'^* = \mathbf{1}^T \mathbf{x} = \mathbf{1}^T \mathbf{x}^*$. This contradicts that $\mathbf{x}^*$ is an optimal RAV with the minimum number of positive elements.

A.3   Proof of Proposition 7

The proof focuses on the case with $\mathbf{J}_0 = \mathbf{0}$ and the result is applicable to the case with any $\mathbf{J}_0 \succeq \mathbf{0}$. Let $\mathbf{x}^*$ denote an optimal solution for $\mathcal{P}$ with the minimum number of positive elements and let $m = \|\mathbf{x}^*\|_0$. If $m \leq \text{rank}\{\boldsymbol{\Lambda}\}$, the proof is completed. We next show that $m > \text{rank}\{\boldsymbol{\Lambda}\}$ will lead to contradiction.

Without loss of generality, consider that the first m elements in $\mathbf{x}^*$ are positive, i.e.,

$$\mathbf{x}^* = [\mathbf{x}^T \ \mathbf{0}_{n-m}^T]^T. \tag{A.3}$$

Let $\widetilde{\mathbf{R}} = \text{diag}\{\xi_1, \xi_2, \cdots, \xi_m\}$ and $\widetilde{\boldsymbol{\Lambda}}$ is the first principle $m \times m$ matrix of $\boldsymbol{\Lambda}$, i.e.,

$$\widetilde{\boldsymbol{\Lambda}} = \mathbf{1}\,\mathbf{1}^T - \widetilde{\mathbf{c}}\,\widetilde{\mathbf{c}}^T - \widetilde{\mathbf{s}}\,\widetilde{\mathbf{s}}^T$$

with

$$\widetilde{\mathbf{c}} = [\cos \phi_1 \ \cos \phi_2 \ \cdots \ \cos \phi_m]^T$$

$$\widetilde{\mathbf{s}} = [\sin \phi_1 \ \sin \phi_2 \ \cdots \ \sin \phi_m]^T.$$

68

Lemma 3. If $\mathbf{y} = \mathbf{x} + \left(\mathbf{I} - \widetilde{\mathbf{R}}^{-1}\widetilde{\boldsymbol{\Lambda}}^{+}\widetilde{\boldsymbol{\Lambda}}\widetilde{\mathbf{R}} \right)\mathbf{w}$, where $\mathbf{x}$ is the vector consisting of the first m elements of $\mathbf{x}^{*}$ in (A.3), and $\mathbf{w}$ is an arbitrary real vector satisfying $\mathbf{y} \succeq \mathbf{0}$, then $\mathbf{y}^{*} = [\, \mathbf{y}^{\mathrm{T}} \ \ \mathbf{0}_{n-m}^{\mathrm{T}}\,]^{\mathrm{T}}$ is an optimal RAV for $\mathscr{P}$.

Proof. To prove $\mathbf{y}^{*}$ is an optimal RAV for $\mathscr{P}$, it suffices to prove that $\mathbf{y}^{*}$ achieves the same SPEB as $\mathbf{x}^{*}$ and that $\mathbf{x}^{*}$ satisfies the total resource constraint.

One can verify that $\mathrm{span}\{\mathbf{1}, \widetilde{\mathbf{c}}, \widetilde{\mathbf{s}}\} = \mathrm{span}\{\text{columns of } \widetilde{\boldsymbol{\Lambda}}\}$ and hence $\mathbf{1}^{\mathrm{T}}(\mathbf{I}-\widetilde{\boldsymbol{\Lambda}}^{+}\widetilde{\boldsymbol{\Lambda}}) = \mathbf{0}^{\mathrm{T}}$. Consequently,

$$\mathbf{1}^{\mathrm{T}}\widetilde{\mathbf{R}}\left(\mathbf{I} - \widetilde{\mathbf{R}}^{-1}\widetilde{\boldsymbol{\Lambda}}^{+}\widetilde{\boldsymbol{\Lambda}}\widetilde{\mathbf{R}} \right) = \mathbf{0}^{\mathrm{T}} \tag{A.4}$$

Note that

$$\mathbf{1}_{n}^{\mathrm{T}}\mathbf{R}\mathbf{x}^{*} \stackrel{(a)}{=} \mathbf{1}_{m}^{\mathrm{T}}\widetilde{\mathbf{R}}\mathbf{x} \stackrel{(b)}{=} \mathbf{1}_{m}^{\mathrm{T}}\widetilde{\mathbf{R}}\mathbf{y} \stackrel{(c)}{=} \mathbf{1}_{n}^{\mathrm{T}}\mathbf{R}\mathbf{y}^{*} \tag{A.5}$$

where (a) is due to the relationship between $\mathbf{x}^{*}$ and $\mathbf{x}$, (b) is due to (A.4), and (c) is due to the relationship between $\mathbf{y}$ and $\mathbf{y}^{*}$.

By the definition of Moore-Penrose pseudo-inverse, $\widetilde{\boldsymbol{\Lambda}}(\mathbf{I} - \widetilde{\boldsymbol{\Lambda}}^{+})\widetilde{\boldsymbol{\Lambda}} = \mathbf{0}$. Consequently,

$$\widetilde{\mathbf{R}}\widetilde{\boldsymbol{\Lambda}}\widetilde{\mathbf{R}}\left(\mathbf{I} - \widetilde{\mathbf{R}}^{-1}\widetilde{\boldsymbol{\Lambda}}^{+}\widetilde{\boldsymbol{\Lambda}}\widetilde{\mathbf{R}} \right) = \mathbf{0} \tag{A.6}$$

Note that

$$\mathbf{x}^{*\mathrm{T}}\mathbf{R}\boldsymbol{\Lambda}\mathbf{R}\mathbf{x}^{*} \stackrel{(d)}{=} \mathbf{x}^{\mathrm{T}}\widetilde{\mathbf{R}}\widetilde{\boldsymbol{\Lambda}}\widetilde{\mathbf{R}}\mathbf{x} \stackrel{(e)}{=} \mathbf{y}^{\mathrm{T}}\widetilde{\mathbf{R}}\widetilde{\boldsymbol{\Lambda}}\widetilde{\mathbf{R}}\mathbf{y} \stackrel{(f)}{=} \mathbf{y}^{*\mathrm{T}}\mathbf{R}\boldsymbol{\Lambda}\mathbf{R}\mathbf{y}^{*} \tag{A.7}$$

where (d) is due to the relationship between $\mathbf{x}$ and $\mathbf{x}^{*}$, (e) is due to (A.6), and (f) is due to the relationship between $\mathbf{y}$ and $\mathbf{y}^{*}$. Equations (A.5) and (A.7) imply that $\mathcal{P}(\mathbf{x}^{*}) = \mathcal{P}(\mathbf{y}^{*})$. As with the analysis in Appendix A.2, $\mathbf{1}^{\mathrm{T}}\mathbf{x} \neq \mathbf{1}^{\mathrm{T}}\mathbf{y}$ leads to a contradiction. Therefore, $\mathbf{1}^{\mathrm{T}}\mathbf{x}^{*} = \mathbf{1}^{\mathrm{T}}\mathbf{x} = \mathbf{1}^{\mathrm{T}}\mathbf{y} = \mathbf{1}^{\mathrm{T}}\mathbf{y}^{*}$, indicating $\mathbf{y}^{*}$ satisfy the total resource constraint and hence the proof is completed. $\qquad\square$

Note that $m > \mathrm{rank}\{\boldsymbol{\Lambda}\} \geq \mathrm{rank}\{\widetilde{\boldsymbol{\Lambda}}\}$, which gives $\mathbf{I} - \widetilde{\boldsymbol{\Lambda}}^{+}\widetilde{\boldsymbol{\Lambda}} \neq \mathbf{0}$, and equivalently,

$\left(\mathbf{I} - \widetilde{\mathbf{R}}^{-1} \widetilde{\mathbf{\Lambda}}^{+} \widetilde{\mathbf{\Lambda}} \widetilde{\mathbf{R}} \right) \neq \mathbf{0}$. Suppose its lth is not $\mathbf{0}$. Consider the following mapping

$$h(t) = \mathbf{x} + \left(\mathbf{I} - \widetilde{\mathbf{R}}^{-1} \widetilde{\mathbf{\Lambda}}^{+} \widetilde{\mathbf{\Lambda}} \widetilde{\mathbf{R}} \right) \cdot \mathbf{e}_l \cdot t$$

where $\mathbf{e}_l \in \mathbb{R}^m$. Lemma 2 implies that there exists t_1 such that (1) $h(t_1) \succeq \mathbf{0}$ and (2) $\|h(t_1)\|_0 < m$. Consider $\widetilde{\mathbf{x}} = [\, h(t_1)^{\mathrm{T}} \, \mathbf{0}^{\mathrm{T}} \,]^{\mathrm{T}}$. By lemma 3, $\widetilde{\mathbf{x}}$ is an optimal RAV for $\mathscr{P}$ and $\|\widetilde{\mathbf{x}}\|_0 < m$. This contradicts the assumption that $\mathbf{x}^*$ is an optimal RAV with the minimum number of positive elements.

A.4 Algebraic Method for Optimal Strategy in Simple Networks

The solution of $\mathscr{P}$ with $\mathbf{J}_0 = \mathbf{0}$ in simple networks is first presented. Note that when $\mathbf{J}_0 = \mathbf{0}$, the SPEB is

$$\mathcal{P}(\mathbf{x}) = \frac{4 \cdot \mathbf{1}^{\mathrm{T}} \mathbf{R} \mathbf{x}}{\mathbf{x}^{\mathrm{T}} \mathbf{R}^{\mathrm{T}} \mathbf{\Lambda} \mathbf{R} \mathbf{x}} =: \widetilde{\mathcal{P}}(\mathbf{x})$$

Proposition 13. If the following conditions hold

$$\begin{cases} \operatorname{rank}\{\mathbf{\Lambda}\} = 3 \\ \mathbf{1}^{\mathrm{T}} (\mathbf{R}\mathbf{\Lambda}\mathbf{R})^{-1} \mathbf{1} > 0 \\ (\mathbf{R}\mathbf{\Lambda}\mathbf{R})^{-1} (\mathbf{R}\mathbf{1} + c\,\mathbf{1}) \succ \mathbf{0} \end{cases} \tag{A.8}$$

where

$$c = \sqrt{1/(\mathbf{1}^{\mathrm{T}} (\mathbf{R}\mathbf{\Lambda}\mathbf{R})^{-1} \mathbf{1})} \tag{A.9}$$

then there exists a unique optimal RAV for $\mathscr{P}$, given by

$$\mathbf{x}^* = \frac{A}{2c} (\mathbf{R}\mathbf{\Lambda}\mathbf{R})^{-1} (\mathbf{R}\mathbf{1} + c\,\mathbf{1}) \tag{A.10}$$

where

$$A = \frac{2c}{\mathbf{1}^{\mathrm{T}}(\mathbf{R}\mathbf{\Lambda}\mathbf{R})^{-1}(\mathbf{R}\mathbf{1} + c\mathbf{1})} \tag{A.11}$$

and the corresponding SPEB $\mathcal{P}(\mathbf{x}^*) = 2 \cdot \mathbf{1}^{\mathrm{T}}(\mathbf{R}\mathbf{\Lambda}\mathbf{R})^{-1}(\mathbf{R}\mathbf{1} + c\mathbf{1})$. Otherwise, there exists an optimal RAV for $\mathscr{P}$ with at most two positive elements.

Proof. See Appendix A.5. □

Proposition 13 provides an efficient method to check if the minimum number of active transmitting nodes is three, and if so, then it provides the optimal RAV for $\mathscr{P}$ analytically.

The closed-form strategy for $\mathscr{P}$ in simple networks is given as follows. Let s_e : $\mathcal{N}_b \times \mathcal{N}_b \to \mathbb{R}$ denote the function

$$s_e(i, j) = \frac{(1/\sqrt{\xi_i} + 1/\sqrt{\xi_j})^2}{\sin^2(\phi_i - \phi_j)}$$

in which $i, j \in \mathcal{N}_b$. Two strategies are provided as follows.

- π_1: the optimal solution is given by (A.10);

- π_2: let $(k_1, k_2) = \arg\min_{\{i,j\}} s_e(i, j)$ and k_3 is the remaining anchor, the RAV is

$$x_{k_1} = \frac{\sqrt{\xi_{k_2}}}{\sqrt{\xi_{k_1}} + \sqrt{\xi_{k_2}}}, \quad x_{k_2} = \frac{\sqrt{\xi_{k_1}}}{\sqrt{\xi_{k_1}} + \sqrt{\xi_{k_2}}}, \quad x_{k_3} = 0.$$

Proposition 14. For a simple network with $\mathbf{J}_0 = \mathbf{0}$, if the conditions in (A.8) hold, the optimal resource allocation strategy $\pi^* = \pi_1$, otherwise $\pi^* = \pi_2$. Moreover, the SPEB is given by

$$\mathcal{P}(\mathbf{x}^*) = \begin{cases} \dfrac{4c}{A} & \text{if } \pi^* = \pi_1 \\[2mm] \min_{\{i,j\}} s_e(i, j) & \text{if } \pi^* = \pi_2 \end{cases}$$

Proof. If conditions in (A.8) hold, π_1 is an optimal strategy by the proof of Proposition 13. Otherwise, there exists an optimal strategy that requires two active anchors.

Suppose anchors i and j are active, then

$$\begin{aligned}
\mathcal{P}(\mathbf{x}) &= \frac{x_i \xi_i + x_j \xi_j}{x_i x_j \, \xi_i \xi_j \sin^2(\phi_i - \phi_j)} \\
&= \frac{1}{\sin^2(\phi_i - \phi_j)} \Big(\frac{1}{\xi_i x_i} + \frac{1}{\xi_j x_j} \Big) \\
&= \frac{x_i + x_j}{\sin^2(\phi_i - \phi_j)} \Big(\frac{1}{\xi_i x_i} + \frac{1}{\xi_j x_j} \Big) \\
&\geq s_e(i, j).
\end{aligned}$$

The last inequality is due to Cauchy-Schwarz inequality and the equality holds iff $x_i = x_j \sqrt{\xi_j / \xi_i}$. Minimizing $s_e(i,j)$ over i, j leads to $(i^*, j^*) = \arg\min_{\{i,j\}} s_e(i, j)$ and thus anchors i^* and j^* are active. $\square$

The solution for $\mathscr{P}$ with $\mathbf{J}_0 \neq \mathbf{0}$ is presented as follows. Though the problem $\mathscr{P}$ for simple networks can be obtained by checking the KKT conditions, the procedure is very complex due to the complicated expression of the SPEB. Hence, the following method, referred to as *prior knowledge decomposition*, is proposed to solve $\mathscr{P}$.

Lemma 4 (Prior Knowledge Decomposition). For an arbitrary symmetric $\mathbf{J}_0$ and a simple network, rank$\{\mathbf{\Lambda}\} = 3$ implies rank$\{\mathbf{\Lambda}_e\} = 3$, where

$$\mathbf{\Lambda}_e = \mathbf{P} \begin{bmatrix} 1 & \mathbf{c} & \mathbf{s} \end{bmatrix}^\mathrm{T} \mathbf{R}$$

in which

$$\mathbf{P} = \begin{bmatrix} 1/2 & 1/2 & 0 \\ 0 & 0 & 1/2 \\ 1/2 & -1/2 & 0 \end{bmatrix}.$$

Moreover, if rank$\{\mathbf{\Lambda}_e\} = 3$, then the vector

$$\mathbf{x}_0 = \mathbf{\Lambda}_e^{-1} \begin{bmatrix} [\mathbf{J}_0]_{11} & [\mathbf{J}_0]_{12} & [\mathbf{J}_0]_{22} \end{bmatrix}^\mathrm{T}$$

satisfies that

$$\mathbf{J}_0 = \sum_{k \in \mathcal{N}_b} [\mathbf{x}_0]_k \, \xi_k \, \mathbf{J}_r(\phi_k).$$ (A.12)

Proof. If rank$\{\boldsymbol{\Lambda}\} = 3$, then $\mathbf{1}$, $\mathbf{c}$ and $\mathbf{s}$ are linearly independent. Note that both $\mathbf{P}$ and $\mathbf{R}$ are invertible. Hence rank$\{\boldsymbol{\Lambda}_e\} = 3$.

The second claim can be verified after some calculation. $\qquad\square$

Lemma 4 shows that if rank$\{\boldsymbol{\Lambda}\} = 3$, the prior positional knowledge can be viewed as localization information obtained by allocating certain (possibly negative) resources to the existing anchors.

If rank$\{\boldsymbol{\Lambda}\} = 3$, $\mathbf{J}_0$ can be decomposed as (A.12). Let $\tilde{\mathbf{x}} = \mathbf{x} + \mathbf{x}_0$, then the SPEB with prior positional knowledge is given by

$$\mathcal{P}(\mathbf{x}) = \widetilde{\mathcal{P}}(\tilde{\mathbf{x}}) = \frac{4 \cdot \mathbf{1}^T \mathbf{R} \, \tilde{\mathbf{x}}}{\tilde{\mathbf{x}}^T \mathbf{R}^T \boldsymbol{\Lambda} \mathbf{R} \, \tilde{\mathbf{x}}}.$$

Consider an ancillary resource allocation problem:

$$\widetilde{\mathscr{P}} : \quad \min_{\{\tilde{\mathbf{x}}\}} \quad \widetilde{\mathcal{P}}(\tilde{\mathbf{x}})$$

$$\text{s.t.} \quad \mathbf{1}^T \cdot \tilde{\mathbf{x}} \leq 1 + \mathbf{1}^T \cdot \mathbf{x}_0$$

$$\tilde{\mathbf{x}} \succeq \mathbf{x}_0.$$

If $\tilde{\mathbf{x}}^*$ is an optimal RAV for $\widetilde{\mathscr{P}}$, then $\mathbf{x}^* = \tilde{\mathbf{x}}^* - \mathbf{x}_0$ is an optimal RAV for $\mathscr{P}$. The objective function of $\widetilde{\mathscr{P}}$ has a simple expression. Therefore, previous results for $\mathbf{J}_0 = \mathbf{0}$ can be used to derive the solution for $\widetilde{\mathscr{P}}$.

Proposition 15. If the following conditions hold

$$\begin{cases} \text{rank}\{\boldsymbol{\Lambda}\} = 3 \\ \mathbf{1}^T (\mathbf{R}\boldsymbol{\Lambda}\mathbf{R})^{-1} \mathbf{1} > 0 \\ A(\mathbf{R}\boldsymbol{\Lambda}\mathbf{R})^{-1}(\mathbf{R}\mathbf{1} + c\,\mathbf{1}) \succ 2c\,(1 + \mathbf{1}^T \cdot \mathbf{x}_0)\,\mathbf{x}_0 \end{cases}$$ (A.13)

73

where c and A are given by (A.9) and (A.11), and $\mathbf{x}_0$ is given by (A.12), then there exists a unique optimal RAV for $\mathscr{P}$, given by

$$\mathbf{x}^* = \frac{A\left(1 + \mathbf{1}^{\mathrm{T}} \cdot \mathbf{x}_0\right)}{2c} \left(\mathbf{R}\boldsymbol{\Lambda}\mathbf{R}\right)^{-1}\left(\mathbf{R}\mathbf{1} + c\,\mathbf{1}\right) - \mathbf{x}_0 \tag{A.14}$$

and the corresponding SPEB $\mathcal{P}(\mathbf{x}^*) = 2 \cdot \mathbf{1}^{\mathrm{T}}(\mathbf{R}\boldsymbol{\Lambda}\mathbf{R})^{-1}(\mathbf{R}\mathbf{1} + c\,\mathbf{1})/(1 + \mathbf{1}^{\mathrm{T}}\mathbf{x}_0)$. Otherwise, there exists an optimal solution for $\mathscr{P}$ with at most two positive elements.

Proof. If the conditions in (A.13) hold, one can decompose $\mathbf{J}_0$ and obtain $\mathbf{x}_0$ in (A.12). For problem $\widetilde{\mathscr{P}}$, similar to the derivation in Appendix A.5, one can verify that there exists a unique optimal RAV $\widetilde{\mathbf{x}}^*$ for $\widetilde{\mathscr{P}}$, given by

$$\widetilde{\mathbf{x}}^* = \frac{A\left(1 + \mathbf{1}^{\mathrm{T}} \cdot \mathbf{x}_0\right)}{2c} \left(\mathbf{R}\boldsymbol{\Lambda}\mathbf{R}\right)^{-1}\left(\mathbf{R}\mathbf{1} + c\,\mathbf{1}\right)$$

where c and A are given by (A.9) and (A.11). Therefore, $\mathbf{x}^* = \widetilde{\mathbf{x}}^* - \mathbf{x}_0$ is the unique optimal RAV for $\mathscr{P}$. If the conditions in (A.13) do not hold, then either rank$\{\boldsymbol{\Lambda}\} = 3$ or rank$\{\boldsymbol{\Lambda}\} \le 2$. For the former, one can decompose $\mathbf{J}_0$ and verify that there exists an optimal RAV for $\mathscr{P}$ with at most two positive elements using the similar derivation in Appendix A.5; for the latter, the proof is completed by Proposition 7. $\square$

Next the case where at most two anchors are required to achieve the minimum SPEB for $\mathscr{P}$ is presented.

Proposition 16. For a network with three anchors (i.e., $\mathcal{N}_{\mathrm{b}} = \{1, 2, 3\}$) where the conditions in (A.13) do not hold, if there exist $\mathbf{x}$ and i, j, k such that

$$C_j\xi_i - C_i\xi_j - E_{i,j} = (2x_j^2\xi_i\xi_j^2 - 2x_i^2\xi_i^2\xi_j)\sin^2(\phi_i - \phi_j) \tag{A.15}$$

$$x_i + x_j = 1, \; x_i > 0, \; x_j > 0, \; x_k = 0 \tag{A.16}$$

$$\frac{\partial}{\partial x_i}\mathcal{P}(\mathbf{x}) < \frac{\partial}{\partial x_k}\mathcal{P}(\mathbf{x}) \tag{A.17}$$

where

$$C_i = 2\xi_i\left(\mathrm{tr}\{\mathbf{J}_0\} + ([\mathbf{J}_0]_{22} - [\mathbf{J}_0]_{11})\cos\phi_i + 4[\mathbf{J}_0]_{12}\sin\phi_i\right)$$

74

$$E_{i,j} = \text{tr}\{\mathbf{J}_0\}\big(2\xi_i\xi_j(x_j - x_i)\sin^2(\phi_i - \phi_j) + C_i - C_j\big)$$

then the optimal RAV for $\mathscr{P}$ is given by $\mathbf{x}$. Otherwise, there exists an optimal RAV for $\mathscr{P}$ with only one non-zero element.

The proof of Proposition 16 is obtained by checking the KKT conditions. Combining (A.15) and (A.16) gives a quadratic equation of x_i and this equation can be solved analytically to achieve $\mathbf{x}$; then one can check whether the inequality (A.17) holds.

The optimal RAV for $\mathscr{P}$ in simple networks is provided as follows:

- Conditions (A.13) hold: the optimal RAV $\mathbf{x}^*$ is given by (A.14);

- Conditions (A.13) do not hold:

    - if there exists $\mathbf{x}$ such that (A.15) to (A.17) hold, then RAV $\mathbf{x}^* = \mathbf{x}$;

    - Otherwise, the optimal RAV for $\mathscr{P}$ has one non-zero element and the optimal RAV can be obtained by checking three anchors one by one.

A.5 Proof of Proposition 13

The RAV $\mathbf{x}^*$ is an optimal solution for $\mathscr{P}$ iff it satisfies KKT conditions

$$\begin{cases} \nabla\mathcal{P}(\mathbf{x}^*) - \boldsymbol{\mu} + \nu \cdot \nabla(\mathbf{1}^\mathsf{T}\mathbf{x}^* - 1) = \mathbf{0} \\[2mm] \mathbf{x}^* \succeq \mathbf{0}, \ \boldsymbol{\mu} \succeq \mathbf{0}, \ \mu_k x_k^* = 0, \ \ k = 1, 2, 3 \\[2mm] \mathbf{1}^\mathsf{T}\mathbf{x}^* = 1 \end{cases}$$

If conditions (A.8) hold, one can verify that the RAV provided in (A.10) satisfies the KKT conditions above with $\boldsymbol{\mu} = \mathbf{0}$. The uniqueness is shown as follows. Suppose there exists another optimal RAV $\tilde{\mathbf{x}}^*$ for $\mathscr{P}$; then $\|\tilde{\mathbf{x}}^*\|_0 = 3$ or $\|\tilde{\mathbf{x}}^*\|_0 \leq 2$.

If $\|\tilde{\mathbf{x}}^*\|_0 = 3$, then $\mu_j = 0, \ j = 1, 2, 3$. Checking KKT conditions with respect to

$\widetilde{\mathbf{x}}^*$, one can obtain

$$\widetilde{\mathbf{x}}^* = \frac{A}{2c}\,(\mathbf{R}\boldsymbol{\Lambda}\mathbf{R})^{-1}(\mathbf{R1} + c\,\mathbf{1}) \tag{A.18}$$

where $A = \widetilde{\mathbf{x}}^{*\mathrm{T}}\,\mathbf{R}\boldsymbol{\Lambda}\mathbf{R}\,\widetilde{\mathbf{x}}^*$ and $c = (\mathbf{R1})^{\mathrm{T}}\,\widetilde{\mathbf{x}}^*$. Substituting (A.18) into $\mathbf{1}^{\mathrm{T}}\mathbf{x}^* = 1$ gives

$$c = \sqrt{\frac{(\mathbf{R1})^{\mathrm{T}}\,(\mathbf{R}\boldsymbol{\Lambda}\mathbf{R})^{-1}\,\mathbf{R1}}{\mathbf{1}^{\mathrm{T}}(\mathbf{R}\boldsymbol{\Lambda}\mathbf{R})^{-1}\mathbf{1}}}, \quad A = \frac{2c}{\mathbf{1}^{\mathrm{T}}(\mathbf{R}\boldsymbol{\Lambda}\mathbf{R})^{-1}(\mathbf{R1} + c\mathbf{1})}.$$

By formulas of trigonometric functions, $(\mathbf{R1})^{\mathrm{T}}\,(\mathbf{R}\boldsymbol{\Lambda}\mathbf{R})^{-1}\,\mathbf{R1} = 1$, and hence c can be simplified as (A.9). Consequently, $\widetilde{\mathbf{x}}^*$ in (A.18) is identical to $\mathbf{x}^*$ in (A.10). Moreover, by substituting $\widetilde{\mathbf{x}}^*$ into $\mathcal{P}(\cdot)$, one can show that $\mathcal{P}(\mathbf{x}^*) = 2 \cdot \mathbf{1}^{\mathrm{T}}(\mathbf{R}\boldsymbol{\Lambda}\mathbf{R})^{-1}(\mathbf{R1} + c\mathbf{1})$.

If $\|\widetilde{\mathbf{x}}^*\|_0 \le 2$, consider a linear combination of $\mathbf{x}^*$ and $\widetilde{\mathbf{x}}^*$ with respect to $\delta \in (0, 1)$: $\mathbf{x}_\delta = (1 - \delta)\mathbf{x}^* + \delta\widetilde{\mathbf{x}}^*$. Note that $\|\mathbf{x}_\delta\|_0 = 3$. By the convexity of $\mathcal{P}(\cdot)$, $\mathbf{x}_\delta$ is also an optimal RAV. This statement contradicts that $\mathbf{x}^*$ is a unique RAV with three positive elements. Hence, $\mathbf{x}^*$ is the unique optimal RAV if the conditions in (A.8) hold.

On the other hand, if the conditions in (A.8) do not hold, we claim that there exists an optimal RAV for $\mathscr{P}$ with at most two positive elements. Otherwise, the optimal RAV $\mathbf{x}^*$ for $\mathscr{P}$ has three positive elements.[2] Then by Lemma 7, rank$\{\boldsymbol{\Lambda}\} = 3$ and therefore rank$\{\mathbf{R}\boldsymbol{\Lambda}\mathbf{R}\} = 3$. KKT conditions imply $\mathbf{x}^* = \frac{A}{2c}\,(\mathbf{R}\boldsymbol{\Lambda}\mathbf{R})^{-1}(\mathbf{R1}+c\,\mathbf{1})$, where c and A are given in (A.9) and (A.11). Since c is a real number, $\mathbf{1}^{\mathrm{T}}\,(\mathbf{R}\boldsymbol{\Lambda}\mathbf{R})^{-1}\mathbf{1} > 0$. Moreover, since $A/2c = 2/\mathcal{P}(\mathbf{x}) > 0$, $\mathbf{x}^* \succ \mathbf{0}$ implies $(\mathbf{R}\boldsymbol{\Lambda}\mathbf{R})^{-1}(\mathbf{R1} + c\,\mathbf{1}) \succ \mathbf{0}$. Then all conditions in (A.8) hold, which contradicts the assumption that the conditions in (A.8) do not hold.

A.6   Proof of Proposition 10

The proof can be divided into two cases that depend on the position of $\mathbf{y}^*$ relative to $\mathcal{I}$: 1) $\mathbf{y}^*$ is an interior point of a face f^* of $\mathcal{I}$ and 2) $\mathbf{y}^*$ lies in an edge of $\mathcal{I}$. The proof focuses on the first case and the result can be easily extended to the second case.

The following lemma can be used for checking the visibility of face.

---

[2]If there are more than one optimal RAV, each of them has three positive elements.

Lemma 5. Given a facet $\tilde{f}$ of a convex polyhedron $\mathcal{C}$ and a point p. $\tilde{f}$ is visible from p iff $\langle \mathbf{n}, \mathbf{h} \rangle < 0$, where $\mathbf{n}$ denotes the outward-pointing normal vector of $\tilde{f}$ and $\mathbf{h}$ is a vector from p to an arbitrary point in $\tilde{f}$.

Lemma 5 can be verified directly from the definition. Let $\mathbf{h}^* = [\, y_1^*, \, y_2^*, \, y_3^* - \mu\,]^\mathrm{T}$ denote the vector from $\mathbf{y}_\mu$ to $\mathbf{y}^*$. Since $\mathbf{y}^*$ is an interior point of f^*, normal vectors of f^* and that of the hyperboloid (3.3) are aligned at $\mathbf{y}^*$, implying that the outward-pointing normal vector of f^* can be written as

$$\mathbf{n}^* = t\,[\,-y_1^*, \, -y_2^*, \, y_3^* - 2/\lambda^*\,]^\mathrm{T}.$$

where $\lambda^* = \mathcal{P}(\mathbf{x}^*) > 0$ and t is a constant. Note that $-\mathbf{n}^*$, the outward-pointing normal vector of (3.3), satisfies that $-n_3^* \leq 0$, implying that

$$t(y_3^* - 2/\lambda^*) \geq 0. \tag{A.19}$$

Moreover, note that $y_3 = \mathbf{1}^\mathrm{T}\mathbf{R}\,\mathbf{x} + \mathrm{tr}\{\mathbf{J}_0\} > 0$ and

$$(y_3^* - 2/\lambda^*)^2 = y_1^{*2} + y_2^{*2} + 4/\lambda^{*2} \geq 4/\lambda^{*2}$$

which gives

$$y_3^* \geq 4/\lambda^*. \tag{A.20}$$

Together with (A.19), this shows that $t > 0$. Without loss of generality, we consider $t = 1$. Then the inner product of $\mathbf{n}^*$ and $\mathbf{h}^*$ is

$$\langle \mathbf{n}^*, \mathbf{h}^* \rangle = -y_1^{*2} - y_2^{*2} + y_3^{*2} - \mu y_3^* - 2y_3^*/\lambda^* + 2\mu/\lambda^*$$
$$\overset{(a)}{=} \mu(2/\lambda^* - y_3^*) + 2y_3^*/\lambda^*$$

where (a) is due to the fact that $\mathbf{y}^*$ is on the curve (3.3). Note that $y_3^* > 2/\lambda^* > 0$ according to (A.20), and hence $\mu(2/\lambda^* - y_3^*) > 0$ and $2y_3^*/\lambda^* > 0$. Consequently,

$\langle \mathbf{n}^*, \mathbf{h}^* \rangle > 0$ and f is not visible from the point $\mathbf{y}_\mu$.

A.7 Proof of the claim in Chapter 6

The following lemma shows that $\mathcal{I}_\mathrm{B}$ is a translate of $\widetilde{\mathcal{I}}_\mathrm{B}$.

Lemma 6. There exists a constant $\mathbf{d}$ such that $\mathcal{I}_\mathrm{B} = \widetilde{\mathcal{I}}_\mathrm{B} + \mathbf{d}$.

Proof. This lemma can be proved by induction. For $N = 2$, $\mathcal{I}_\mathrm{B}$ obtained by Line 1 to Line 3 in Algorithm 4 is a parallelogram, and its edges (in a clockwise order) are either $(\mathbf{y}_1, \mathbf{y}_2, -\mathbf{y}_1, -\mathbf{y}_2)$ or $(\mathbf{y}_1, -\mathbf{y}_2, -\mathbf{y}_1, \mathbf{y}_2)$, depending on the angles of $\mathbf{y}_1$ and $\mathbf{y}_2$. In either case, there exists a constant $\mathbf{d}^{(2)}$ such that $\mathcal{I}_\mathrm{B} = \widetilde{\mathcal{I}}_\mathrm{B} + \mathbf{d}^{(2)}$.

Let

$$\mathcal{I}_\mathrm{B}^{(i)} = \left\{ \sum_{k=1}^{i} c_k \mathbf{y}_k : 0 \le c_k \le 1 \right\}$$

and let $\widetilde{\mathcal{I}}_\mathrm{B}^{(i)}$ denote the polygon obtained by Line 1 to Line 3 in Algorithm 4 with input vectors $\mathbf{y}_1, \mathbf{y}_2, \cdots, \mathbf{y}_i$. Note that $\mathcal{I}_\mathrm{B} = \mathcal{I}_\mathrm{B}^{(N)}$ and $\widetilde{\mathcal{I}}_\mathrm{B} = \widetilde{\mathcal{I}}_\mathrm{B}^{(N)}$.

Suppose the lemma is proved for $N = l - 1$. The induction hypothesis implies that there exists a constant $\mathbf{d}^{(l-1)}$ such that $\mathcal{I}_\mathrm{B}^{(l-1)} = \widetilde{\mathcal{I}}_\mathrm{B}^{(l-1)} + \mathbf{d}^{(l-1)}$. Consider the case $N = l$. Note that

$$\mathcal{I}_\mathrm{B}^{(l)} = \left\{ \mathbf{y} : \mathbf{y} = t \cdot \mathbf{y}_l + \mathbf{z}, \mathbf{z} \in \mathcal{I}_\mathrm{B}^{(l-1)}, 0 \le t \le 1 \right\} \tag{A.21}$$

and

$$\widetilde{\mathcal{I}}_\mathrm{B}^{(l)} = \left\{ \mathbf{y} : \mathbf{y} = t \cdot \mathbf{y}_l + \widetilde{\mathbf{z}} + \mathbf{r}, \widetilde{\mathbf{z}} \in \widetilde{\mathcal{I}}_\mathrm{B}^{(l-1)}, 0 \le t \le 1 \right\} \tag{A.22}$$

for some constant $\mathbf{r}$ that depends on $\mathbf{y}_l$ and $\widetilde{\mathcal{I}}_\mathrm{B}^{(l-1)}$. Comparing (A.21) and (A.22) shows that $\mathcal{I}_\mathrm{B}^{(l)} = \widetilde{\mathcal{I}}_\mathrm{B}^{(l)} + \mathbf{d}^{(l)}$, where $\mathbf{d}^{(l)} = \mathbf{d}^{(l-1)} - \mathbf{r}$. $\qquad\square$

Next consider the point in $\mathcal{I}_\mathrm{B}$ with the largest x-component, denoted as $\mathbf{y}_\mathrm{r}$. This point is unique since none of the vectors $\mathbf{y}_1, \mathbf{y}_2, \cdots, \mathbf{y}_N$ is parallel to the vertical

axis. Therefore, $\mathcal{I}_{\mathrm{B}}$ can be obtained by translating $\widetilde{\mathcal{I}}_{\mathrm{B}}$ so that $\widetilde{\mathbf{y}}_{\mathrm{R}}$ overlaps $\mathbf{y}_{\mathrm{r}}$. The only thing remaining to show is that $\mathbf{y}_{\mathrm{r}}$ is identical to the point $\mathbf{y}_{\mathrm{R}}$ obtained in Line 4 and Line 5. Let $X(\mathbf{y})$ denote the x-component of a 2-D vector $\mathbf{y}$. Then

$$
\begin{aligned}
\mathbf{y}_{\mathrm{r}} &= \arg\max_{\mathbf{y} \in \mathcal{I}_{\mathrm{B}}} \; X(\mathbf{y}) \\
&= \arg\max_{\mathbf{y} = \sum_{i=1}^{N} c_i \mathbf{y}_i, 0 \leq c_i \leq 1} \; X(\mathbf{y}) \\
&= \arg\max_{\mathbf{y} = \sum c_i \mathbf{y}_i, 0 \leq c_i \leq 1, X(\mathbf{y}_i) \geq 0} \; X(\mathbf{y}) \\
&= \sum_{X(\mathbf{y}_i) \geq 0} \mathbf{y}_i \\
&= \mathbf{y}_{\mathrm{R}}.
\end{aligned}
$$

Bibliography

[1] U. A. Khan, S. Kar, and J. M. F. Moura, "Distributed sensor localization in random environments using minimal number of anchor nodes," *IEEE Trans. Signal Process.*, vol. 57, no. 5, pp. 2000–2016, May 2009.

[2] Y. Shen, S. Mazuelas, and M. Z. Win, "Network navigation: Theory and interpretation," *IEEE J. Sel. Areas Commun.*, vol. 30, no. 9, pp. 1823–1834, Oct. 2012. [Online]. Available: http://arxiv.org/abs/1112.3599

[3] K. Plarre and P. R. Kumar, "Tracking objects with networked scattered directional sensors," *EURASIP J. Adv. in Signal Process.*, vol. 2008, no. 74, pp. 1–10, Jan. 2008.

[4] U. A. Khan, S. Kar, and J. M. F. Moura, "DILAND: An algorithm for distributed sensor localization with noisy distance measurements," *IEEE Trans. Signal Process.*, vol. 58, no. 3, pp. 1940–1947, Mar. 2010.

[5] S. Gezici, Z. Tian, G. B. Giannakis, H. Kobayashi, A. F. Molisch, H. V. Poor, and Z. Sahinoglu, "Localization via ultra-wideband radios: A look at positioning aspects for future sensor networks," *IEEE Signal Process. Mag.*, vol. 22, no. 4, pp. 70–84, Jul. 2005.

[6] A. H. Sayed, A. Tarighat, and N. Khajehnouri, "Network-based wireless location: Challenges faced in developing techniques for accurate wireless location information," *IEEE Signal Process. Mag.*, vol. 22, no. 4, pp. 24–40, Jul. 2005.

[7] Y. Shen and M. Z. Win, "Fundamental limits of wideband localization – Part I: A general framework," *IEEE Trans. Inf. Theory*, vol. 56, no. 10, pp. 4956–4980, Oct. 2010. [Online]. Available: http://arxiv.org/abs/1006.0888v1

[8] J. J. Caffery and G. L. Stuber, "Overview of radiolocation in CDMA cellular systems," *IEEE Commun. Mag.*, vol. 36, no. 4, pp. 38–45, Apr. 1998.

[9] B. Denis, J.-B. Pierrot, and C. Abou-Rjeily, "Joint distributed synchronization and positioning in UWB ad hoc networks using TOA," *IEEE Trans. Microw. Theory Tech.*, vol. 54, no. 4, pp. 1896 – 1911, Jun. 2006.

[10] A. Rabbachin, I. Oppermann, and B. Denis, "GML ToA estimation based on low complexity UWB energy detection," in *Proc. IEEE Int. Symp. on Personal, Indoor and Mobile Radio Commun.*, Helsinki, Finland, Sep. 2006, pp. 1–5.

81

[11] M. Z. Win, A. Conti, S. Mazuelas, Y. Shen, W. M. Gifford, D. Dardari, and M. Chiani, "Network localization and navigation via cooperation," *IEEE Commun. Mag.*, vol. 49, no. 5, pp. 56–62, May 2011.

[12] C.-Y. Chong and S. P. Kumar, "Sensor networks: evolution, opportunities, and challenges," *Proc. IEEE*, vol. 91, no. 8, pp. 1247–1256, Aug. 2003.

[13] K. Pahlavan, X. Li, and J.-P. Mäkelä, "Indoor geolocation science and technology," *IEEE Commun. Mag.*, vol. 40, no. 2, pp. 112–118, Feb. 2002.

[14] H. Godrich, A. M. Haimovich, and R. S. Blum, "Target localization accuracy gain in MIMO radar-based systems," *IEEE Trans. Inf. Theory*, vol. 56, no. 6, pp. 2783–2803, Jun. 2010.

[15] A. M. Haimovich, R. S. Blum, and L. J. Cimini, "MIMO radar with widely separated antennas," *IEEE Signal Process. Mag.*, vol. 25, no. 1, pp. 116–129, Jan. 2008.

[16] E. Paolini, A. Giorgetti, M. Chiani, R. Minutolo, and M. Montanari, "Localization capability of cooperative anti-intruder radar systems," *EURASIP J. Adv. Signal Process.*, vol. 2008, pp. 1–14, Apr. 2008.

[17] L. Mailaender, "On the geolocation bounds for round-trip time-of-arrival and all non-line-of-sight channels," *EURASIP J. Adv. in Signal Process.*, vol. 2008, pp. 1–10, 2008.

[18] Y. Shen, H. Wymeersch, and M. Z. Win, "Fundamental limits of wideband localization – Part II: Cooperative networks," *IEEE Trans. Inf. Theory*, vol. 56, no. 10, pp. 4981–5000, Oct. 2010. [Online]. Available: http://arxiv.org/abs/1006.0890v1

[19] D. B. Jourdan, D. Dardari, and M. Z. Win, "Position error bound for UWB localization in dense cluttered environments," *IEEE Trans. Aerosp. Electron. Syst.*, vol. 44, no. 2, pp. 613–628, Apr. 2008.

[20] Y. Qi, H. Kobayashi, and H. Suda, "Analysis of wireless geolocation in a non-line-of-sight environment," *IEEE Trans. Wireless Commun.*, vol. 5, no. 3, pp. 672–681, Mar. 2006.

[21] D. Dardari, A. Conti, U. J. Ferner, A. Giorgetti, and M. Z. Win, "Ranging with ultrawide bandwidth signals in multipath environments," *Proc. IEEE*, vol. 97, no. 2, pp. 404–426, Feb. 2009, special issue on *Ultra-Wide Bandwidth (UWB) Technology & Emerging Applications*.

[22] F. Meshkati, H. V. Poor, and S. C. Schwartz, "Energy-efficient resource allocation in wireless networks," *IEEE Signal Process. Mag.*, vol. 24, no. 3, pp. 58–68, May 2007.

[23] M. Gorlatova, P. Kinget, I. Kymissis, D. Rubenstein, X. Wang, and G. Zussman, "Energy-Harvesting active networked tags (EnHANTs) for ubiquitous object networking," *IEEE Wireless Commun. Mag.*, vol. 17, no. 6, pp. 18–25, Dec. 2010.

[24] R. K. Ahuja, T. L. Magnanti, and J. B. Orlin, *Network Flows: Theory, Algorithms, and Applications.* Prentice hall, 1993.

[25] F. P. Kelly, A. K. Maulloo, and D. K. H. Tan, "Rate control for communication networks: Shadow prices, proportional fairness and stability," *J. Oper. Res. Soc.*, vol. 49, no. 3, pp. 237–252, Mar. 1998.

[26] S. Boyd and L. Vandenberghe, *Convex Optimization.* Cambridge, UK: Cambridge University Press, 2004.

[27] Z.-Q. Luo and W. Yu, "An introduction to convex optimization for communications and signal processing," *IEEE J. Sel. Areas Commun.*, vol. 24, no. 8, pp. 1426–1438, Aug. 2006.

[28] G. J. Foschini, "Private conversation," AT&T Labs-Research, May 2001, Middletown, NJ.

[29] L. A. Shepp, "Private conversation," AT&T Labs-Research, Mar. 2001, Middletown, NJ.

[30] D. Bertsimas, D. B. Brown, and C. Caramanis, "Theory and applications of robust optimization," *SIAM Rev.*, vol. 53, no. 3, pp. 464–501, Aug. 2011.

[31] W. Dai, Y. Shen, and M. Z. Win, "On the minimum number of active anchors for optimal localization," in *Proc. IEEE Global Telecomm. Conf.*, Anaheim, CA, Dec. 2012, pp. 4951–4956.

[32] ——, "Sparsity-inspired power allocation algorithms for network localization," in *Proc. IEEE Int. Conf. Commun.*, Budapest, Hungary, Jun. 2013, pp. 1378–1383.

[33] Y. Shen, W. Dai, and M. Z. Win, "Power optimization for network localization," *IEEE/ACM Trans. Netw.*, Aug. 2014, to appear.

[34] Y. Shen and M. Z. Win, "Energy efficient location-aware networks," in *Proc. IEEE Int. Conf. Commun.*, Beijing, China, May 2008, pp. 2995–3001.

[35] H. Godrich, A. P. Petropulu, and H. V. Poor, "Power allocation strategies for target localization in distributed multiple-radar architectures," *IEEE Trans. Signal Process.*, vol. 59, no. 7, pp. 3226–3240, Jul. 2011.

[36] T. Wang, G. Leus, and L. Huang, "Ranging energy optimization for robust sensor positioning based on semidefinite programming," *IEEE Trans. Signal Process.*, vol. 57, no. 12, pp. 4777–4787, Dec. 2009.

[37] W. W.-L. Li, Y. Shen, Y. J. Zhang, and M. Z. Win, "Robust power allocation for energy-efficient location-aware networks," *IEEE/ACM Trans. Netw.*, vol. 21, no. 6, pp. 1918–1930, Dec. 2013.

[38] T. M. Chan, "Optimal output-sensitive convex hull algorithms in two and three dimensions," *Discrete and Computational Geometry*, vol. 16, pp. 361–368, 1996.

[39] M. S. Lobo, L. Vandenberghe, S. Boyd, and H. Lebret, "Applications of second-order cone programming," *Linear Algebra and its Applications*, vol. 284, no. 1-3, pp. 193–228, Nov. 1998.

[40] M. de Berg, O. Cheong, M. van Kreveld, and M. Overmars, *Computational Geometry: Algorithms and Applications*. Springer-Verlag, 2008.